**Article:**
Mountney, NP and Hême de Lacotte, VJP (2022) A classification scheme for sedimentary architectures arising from aeolian-fluvial system interactions: Permian examples from southeast Utah, USA. Aeolian Research, 58. 100815. ISSN: 1875-9637

https://doi.org/10.1016/j.aeolia.2022.100815

**A classification scheme for sedimentary architectures arising from aeolian-fluvial system interactions: Permian examples from southeast Utah, USA**

Victor J.P. Hême de Lacotte a,b & Nigel P. Mountney b

a Université de Lyon, UCBL, CNRS, ENSL, LGL-TPE, 69622 Villeurbanne, France
b Fluvial, Eolian & Shallow-Marine Research Group, School of Earth and Environment, University of Leeds, Leeds LS2 9JT, United Kingdom

**ABSTRACT**
The preservation of the sedimentary deposits of arid environments is determined by both geomorphic and geologic processes. Sedimentary evidence of aeolian-fluvial system interactions in arid-climate settings are preserved in both recent and ancient sedimentary successions. However, despite considerable prior sedimentological research, there is no unifying scheme to provide generalized definitions of commonly occurring types of preserved aeolian-fluvial interactions. This study addresses this shortcoming by introducing a novel classification scheme for sedimentary architectures arising from such system interactions. The scheme is demonstrated through reference to examples from the Permian Cutler Group, Paradox Basin, Southeast Utah, USA – a sedimentary record of competing aeolian dune-field and fluvial-fan systems along a palaeo-coastline. Well-preserved, laterally continuous outcrops arranged in different orientations enable three-dimensional architectural characterization. The sedimentary record of eight distinct types of aeolian-fluvial interaction are identified: (i) water-table- controlled interdune sedimentation; (ii) deposits of low-energy fluvial floods; (iii) isolated fluvial channel-fills originating from episodic and confined flooding of interdunes in orientations parallel to the trend of dune crestlines; (iv) channel fills oriented perpendicular to the trend of dune crestlines; (v) amalgamated fluvial channel elements resulting from persistent, long-lived but confined dune-field flooding; (vi) deposits of unconfined sheet-like flood deposits; (vii) fluvial breaching of dunes and their reworking by catastrophic flooding; (viii) aeolian reworking of fluvial deposits. Each interaction type is characterized in terms of preserved sedimentary facies, architectural element geometries and associated proprieties, to demonstrate sedimentary variability in three dimensions. Results provide a guide with which to make sedimentological comparisons and interpretations between active systems and their preserved depositional record.

Keywords: Aeolian Fluvial Dryland Interdune Paradox basin Sedimentary processes

## 1. Introduction

The marginal areas of aeolian dune fields and sand seas (ergs) are prone to numerous geomorphic interactions between sedimentary systems of different types. In places where aeolian dune fields occur in close proximity to mountain fronts or major alluvial plains, dynamic interactions between aeolian and alluvial-fluvial sedimentary systems are common. Numerous case studies provide detailed descriptions of the processes that operate during such interactions. For example, the Skeleton Coast erg in northern Namibia experiences repeated episodes of ponding of water from flash floods by dune damming and termination of fluvial stream networks in interdunes (Teller et al., 1990; Stanistreet & Stollhofen, 2002; Krapf et al., 2003; Svendsen et al., 2003; Feder et al., 2018). Examples of fluvial incursions of the Todd River into the Simpson Desert, Australia, showcase types of fluvial avulsion and sediment reworking by aeolian processes (Hollands et al., 2006). Wet aeolian systems controlled by a high relative water-table level in contact with the accumulation surface are observed in cold, humid, high-latitude settings, e.g., Sólheimasandur (Mountney & Russell, 2006) and Skeiðarársandur (Mountney & Russell, 2009), southern Iceland. Similar interactions are also observed in both arid and humid, low-latitude settings, e.g., North Padre Island, Texas (Hummel & Kocurek, 1984; Kocurek et al., 1992). Interactions between aeolian dunes and ephemeral river systems are common at the margins of many large-scale dune fields in arid environments, including parts of the Rub ʾal Khali of the United Arabic Emirates (Al Farraj & Harvey, 2004), the Wahiba Sands of Oman (Robinson et al., 2007) and the Guandacol Valley of Argentina (Bernárdez et al., 2021). Controls on sediment fluxes between fluvial and aeolian stores have been reviewed (Langford, 1989; Bullard & Livingstone, 2002; Bullard & McTainsh, 2003; Tooth, 2000). Based on analyses of satellite images and aerial photography, several generalized geomorphic classification schemes for modern aeolian-fluvial system interactions have been proposed (e.g., Al-Masrahy & Mountney, 2015; Liu & Coulthard, 2015; Santos et al., 2019).

Compared to present-day systems, there are fewer documented examples of the preserved sedimentary record of aeolian-fluvial system interactions from studies of the ancient geologic record. Nevertheless, several notable studies document a variety of preserved sedimentary architectural relationships interpreted to have arisen from aeolian-fluvial interactions. Preserved fluvial and water-influenced architectural elements nested within otherwise aeolian-dominated successions are recorded from numerous ancient successions (Table 1). In particular, well-preserved sedimentary records of aeolian-fluvial interactions are widely documented from three different stratigraphic groups in the Colorado Plateau region of the southwestern USA, exposed in southern Utah, northern Arizona and western Colorado. Here, research on the Jurassic Glen Canyon and San Rafael groups has revealed various types of such interactions (Kocurek, 1981; Middleton & Blakey, 1983; Clemmensen et al., 1989; Herries, 1993; Jones & Blakey, 1997; Carr-Crabaugh & Kocurek, 1998; Ahmed Benan & Kocurek, 2000; Priddy & Clarke, 2020). In addition, studies of formations that make up the Permian Cutler Group have enabled significant advances in our understanding of the region's palaeoenvironmental history (Loope, 1985; Langford & Chan, 1988, 1989; Stanesco & Campbell, 1989; Mountney & Jagger, 2004; Mountney, 2006a, b; Cain & Mountney, 2009; Taggart et al., 2010; Jordan & Mountney, 2010, 2012; Wakefield and Mountney, 2013). Collectively, these studies demonstrate the diversity of preserved aeolian-fluvial interactions responsible for generating a complex stratigraphic record. However, hitherto, no single unifying scheme has been proposed to classify the broad range of types of aeolian-fluvial interaction known from the rock record.

The aim of this study is to develop and present a unifying and generally applicable classification and interpretation scheme for the preserved sedimentary record of common types of aeolian-fluvial system interaction. Specific research objectives are as follows: (i) to present and describe key attributes of lithofacies and architectural elements (sedimentary characteristics and geometric proprieties) for eight distinct and common types of aeolian-fluvial interaction; (ii) to undertake a statistical analysis of variations in the dimensions of preserved architectural elements and thereby present a summary of their external geometries and their internal sedimentary characteristics; (iii) to explain and discuss the influence of aeolian dune-field geomorphology (e.g., the trend of original dune crestlines and continuity of adjoining interdune corridors) on preserved aeolian-fluvial architectures that form a sedimentary record of aeolian dune-field margin palaeoenvironmental settings; (iv) to highlight how architectural elements accumulated as a result of long-lasting interdune flooding differ from those associated with short-lived floods. These objectives are realized through development of a classification scheme based on the analysis of sedimentary architectures and an associated synthesis of data described in numerous field investigations of the sedimentology and stratigraphy of formations of the Cutler Group in the Paradox Basin, Utah, USA.

***TABLE 1.*** *Notable examples of well-exposed ancient sedimentary formations interpreted to record mixed aeolian-fluvial depositional systems.*

## 2. Geological setting of the Permian Cutler Group, Paradox Basin, USA

Sedimentary successions of the Cutler Group are exposed in the Paradox Basin, south-eastern Utah, USA (Fig. 1). Accumulation of this succession commenced in the late Pennsylvanian, but the succession is mostly of Permian age (Nuccio & Condon, 1996; Rankey, 1997). The stratigraphic fill of the basin is currently revealed by marked fluvial incision of the active Colorado and Green rivers and their tributaries in response to the Neogene to Recent uplift of the Colorado Plateau (Pederson et al., 2002; Liu & Gurnis, 2010). The region records exceptional preservation and laterally continuous exposure; across much of the region; there is no major structural disruption of stratigraphic sections, such that major stratal units and their bounding surfaces can be correlated reliably. Permian units of the Cutler Group record sedimentological conditions that evolved in response to varying climate regimes in several intimately related depositional environments of aeolian, fluvial and lacustrine origin, as well as coastal plain, shoreline and shallow-marine origin (Loope, 1981, 1984). These Permian successions are ideally suited to demonstrating the preserved sedimentary expressions of common types of aeolian-fluvial interaction.

Units of the Cutler Group accumulated mostly under the influence of an arid to semi-arid climate regime (rarely sub-humid) in an evolving and competing aeolian, fluvial and coastal depositional system (Mack, 1979; Loope, 1984). In southeast Utah, the succession comprises four principal formations, in stratigraphic order: the lower Cutler beds, the Cedar Mesa Sandstone, the Organ Rock Formation and the White Rim Sandstone. Although, these units are readily distinguishable in the southern part of the basin, they are considered as one composite succession in its north-eastern part: the Undivided (or Undifferentiated) Cutler Group (Stanesco & Campbell, 1989; Loope et al., 1990).

The lower Cutler beds are defined by the occurrence of fluvial, aeolian and mixed clastic-carbonate shallow-marine facies. These deposits record a tripartite system that evolved in response to repeated eustatic variations (Loope, 1984; Rankey, 1997; Jordan & Mountney, 2010, 2012; Wakefield & Mountney, 2013). Aeolian sedimentation dominated during deposition of the overlying and succeeding Cedar Mesa Sandstone. Sediment accumulation was governed by an aeolian erg system that was, in places, controlled by a water-table level that interacted with the accumulation surface (Loope, 1984, 1985; Langford & Chan, 1988; Jagger, 2003; Mountney & Jagger, 2004). This sedimentary system was characterized by aeolian dunes with a unimodal palaeo-migration direction to the southeast (Loope, 1984; Mountney, 2006b). Periodic deflation of the dunes to the level of the water table occurred, likely in relation to climate change driven by Milankovitch-type cyclicity that affected aeolian sediment supply and its availability for transport (Loope, 1985; Mountney, 2006b; Taggart et al., 2010). Contemporaneous fluvial systems interacted with the aeolian dunes at the margins of the dune field (Langford & Chan, 1988; Mountney & Jagger, 2004). The overlying Organ Rock Formation records the progradation of a terminal fluvial fan – a type of distributive fluvial system – south-westwards, and its downstream passage into the fringe of a contemporaneous aeolian-dominated system (Stanesco & Campbell, 1989; Cain, 2009; Cain & Mountney, 2009, 2011). In the uppermost part of the Cutler Group in parts of southeast Utah, the White Rim Sandstone records a coastal aeolian erg system that was subject to marine transgression (Huntoon & Chan, 1987; Kamola & Chan, 1988; Chan, 1989; Langford & Chan, 1989). In places, the White Rim Sandstone is absent, having been eroded; an unconformity is present at the top of the Permian Cutler Group. Accumulation of the Undivided Cutler Group in the north-eastern part of the basin recorded the activity of a large proximal alluvial fan that occupied much of the evolving foredeep (Nuccio & Condon, 1996; Cain & Mountney, 2009). Collectively, the formations of the Cutler Group exposed in the Paradox Basin provide an opportunity to observe and describe a variety of types of competing aeolian-fluvial interaction.

***FIGURE 1 (2-column fitting).*** *Locations of the main study sites and extent of the Paradox Basin as defined by the distribution of salt deposits of the Paradox Formation that accumulated as an evaporitic marine system in the basin during the Pennsylvanian (Condon, 1997; Stanesco et al., 2000). Map is augmented with data from Wakefield (2010). Elevation data are extracted from the USGS TNM website (https://apps.nationalmap.gov/downloader). Amounts of recorded observations per data source, interaction style and stratigraphic unit are given. Because of the observation scale of FLR elements – centimetre to decimetre, no data are recorded for interaction style 8. Photograph of the typical outcropping sedimentary architecture of the lower Cutler beds (A) and the Cedar Mesa Sandstone – light orange – overlain by the Organ Rock Formation – dark orange (B).*

## 3. Data and methods

Descriptions and interpretations of the sedimentology and stratigraphy of units thought to record types of aeolian-fluvial interaction have been made by analysing data acquired from outcrops of the Cutler Group (lower Cutler beds, Cedar Mesa Sandstone, Organ Rock Formation, White Rim Sandstone and Undivided Cutler Group) in the Paradox Basin. Field-derived sedimentological data were acquired during 20 field campaigns from 1997 to 2019; for details, see Jagger (2003), Mountney & Jagger (2004), Mountney (2006b), Cain (2009) and Wakefield (2010). The data are herein depicted in a series of detailed, scaled two-dimensional drawings of cliff faces portrayed as architectural element panels. We conducted an element inventory through the analysis of 24 high-resolution architectural panels and associated photomosaics, each depicting outcrops of 100 to 2,100 m in lateral

extent, and 9 to 70 m in height. Each panel depicts the geometry of distinct architectural elements and their bounding surfaces, the internal facies units that comprise these elements, and the spatial interrelationships between neighboring elements. In total, 521 discrete architectural elements are recorded. These elements internally comprise 13 sedimentologically distinct lithofacies types (Table 2). These are assigned to 8 architectural element types (Table 3). To assist in establishing the palaeoenvironmental significance of the architectural elements, the following features are also recorded: erosive and conformable bounding surfaces (including aeolian reactivation surfaces, interdune migration surfaces and supersurfaces), sedimentary structures indicative of particular environmental conditions during or shortly after sedimentation (e.g., types and distribution of bioturbation, rhizoliths, nodules and concretions, such as calcrete), types and directions (vertical or lateral) of facies transitions, and palaeocurrent data (Fig. 2; Fig 3).

Architectural elements that arise from aeolian-fluvial interactions are, in part, controlled by the shape and trend of aeolian dunes at the time of deposition. Therefore, the apparent geometries of elements evident in the two-dimensional cross-sections represented by the outcropping cliff faces (and thereby panels depicting those outcrops) record significant variability according to the orientation of the viewed sections with respect to the aeolian dune palaeo-migration direction (Kocurek, 1981). In most cases, key architectural geometries and relationships attributed to each identified type of aeolian-fluvial interaction have been summarized into two types of representative schematic architectural panels: one oriented parallel to the reconstructed aeolian palaeo-transport direction; the other oriented perpendicular (Fig. 2). In cases where sedimentary architectures are considered not to have been influenced by the trend of original aeolian dunes, only one schematic panel is shown. Data represented on the architectural panels were obtained from primary fieldwork by Mountney and supplemented with data presented in Jagger (2003), Cain (2009) and Wakefield (2010). Panels are assigned as *parallel* or *perpendicular* classes, respectively, depending on their orientation relative to the reconstructed aeolian palaeo-transport direction given by Loope (1984) for the lower Cutler beds, Mountney & Jagger (2004) for the Cedar Mesa Sandstone, Cain & Mountney (2009) for the Organ Rock Formation and Undivided Cutler Group, and Huntoon et al. (1987) for the White Rim Sandstone. Importantly, the aeolian palaeo-transport remained largely consistent throughout accumulation of the Cutler Group: the overall regional aeolian dune migration direction was consistently toward 135 degrees (to the southeast). The migrating aeolian dunes have been interpreted previously to have had crestlines oriented close to transverse to the direction of migration (i.e., aligned northeast to southwest; Mountney & Jagger, 2004; Mountney, 2006b). However, the formative palaeo-wind may have blown in varying directions and the resultant bedforms (as expressed by the preserved aeolian dune deposits) may have been oriented slightly oblique to the net wind (Mountney & Jagger, 2004; Mountney, 2006; cf. Rubin & Hunter, 1985, 1987; Rubin & Ideka, 1990).

***TABLE 2.*** *Summary of common lithofacies observed in the studied successions.*

***TABLE 3.*** *Summary of architectural elements representing fluvial-aeolian interactions in the studied successions, and their constituent lithofacies.*

Detailed qualitative description and quantitative analysis of metrics of architectural elements have been undertaken for the data recorded from each of the studied outcrops to identify frequency trends

and statistical characteristics for each type of interaction. The following have been recorded: mean thicknesses and mean widths of architectural elements, a qualitative descriptor of element geometry (e.g., lenticular; laterally continuous), basal element relationship with respect to the underlying unit (e.g., erosive; sharp; gradational; conformable), observation frequencies of sedimentary structures and features, and notable facies associations (Fig. 2). The architectural panels depicting outcrop geometries were originally constructed in an orientation normal to the ground. Given this, and negligible tectonic tilt within the regions of study, recorded element thicknesses represent *true* thicknesses for the points at which they were measured. However, these are not necessarily *maximum* element thicknesses, since it is not usually possible to determine what part of the 3D element is represented in a 2D cross-section. An outcrop plane will not necessarily intersect an element at its point of maximum thickness; for example, the thickness of an interdune-pond element will thin to zero at its margins and will typically be greatest close to its centre. Element thicknesses measured from two-dimensional outcrops are a range of values, which in some cases might include the true maximum thickness, but in other cases will not. Where appropriate, a trigonometric correction has been applied on measured element widths to correct for the angular difference between panel orientations and the determined aeolian palaeo-transport direction. In several cases, the original dimensions of architectural elements could not be determined, either because overlying elements had erosive-bases, else because the lateral limits of elements were not bounded within the studied outcrop section; such unclassified widths cannot be measured in an absolute way; only a minimum unconfined width can be stated (cf. Geehan & Underwood, 1993).

***FIGURE 2 (2-column fitting).*** *A) Example of part of an architectural panel highlighting the different surface boundaries recorded for aeolian-fluvial successions of the Paradox Basin. The architectural panel is depicted normal to the ground; thus, measured thicknesses of architectural elements are true thicknesses for the point of observation. Measured widths are only apparent and depend on the panel orientation relative to the aeolian palaeo-transport direction, and therefore to the orientation of the original aeolian dune bedforms. B) Schematic diagram of a water-table-controlled aeolian system that has accumulated via bedform climbing, with transport-parallel and transport-perpendicular panel views revealing the form of the preserved deposits. C) Simplified inventory of the different sedimentary features, structures, lithofacies and architectural elements examined as part of the present study.*

***FIGURE 3 (2-column fitting).*** *A) transport-perpendicular section of an aeolian dune facies unit (Adu) exhibiting sets of trough cross-bedding as a compound coset, Cedar Mesa Sandstone; B) prominent red mudstone wet interdune pond deposit (WID element) enclosed between Adu units, Cedar Mesa Sandstone; red mudstone bed is 0.25 m thick; C) intertonguing relationship between silty-sandstone deposits of a wet interdune (WID) element and overlying toesets of an aeolian dune (Adu) unit, Cedar Mesa Sandstone; penknife for scale; D) layered chert deposit forming the uppermost part of the fill of a wet interdune (WID) element, Cedar Mesa Sandstone; E) damp interdune (DID) element (arrow indicates position)in a 20 m-thick aeolian sequence, Cedar Mesa Sandstone; F) calcrete palaeosol developed in silty sandstone of a damp interdune (DID) element, Cedar Mesa Sandstone; glove for scale; G) in-situ tree trunk rhizolith preserved in a damp interdune (DID) element, Cedar Mesa Sandstone; penknife for scale; H) bioturbation on a sandstone bedding surface in a damp interdune (DID) element, Cedar Mesa Sandstone; I) adhesion structures preserved on a silty-sandstone bedding surface in a damp interdune (DID) element, Cedar Mesa Sandstone; J) siltstone and fine sandstone (LED element) with current ripples and desiccation cracks between Adu units, Cedar Mesa Sandstone; observed cliff section is 20 m high; K) wave-ripple stratification*

*preserved in a sandstone bed of a LED element, Organ Rock Formation; L) heterolithic strata of an isolated fluvial channel-fill (ICF element) onlapping onto the flanks of a preserved aeolian dune lee; section is oriented perpendicular to aeolian palaeo-transport, which was to the right as viewed; the overlying massive sandstone beds are of an amalgamated channelized (ACF) element; lower Cutler beds; observed cliff section is 20 m high; M) isolated channel-fill (ICF) element with pebble lag filling base of channel; the channel incises into an underlying LED element; Adu units are present a the base and top of the image; lower Cutler beds; observed cliff section is 8 m high; N) linguoid current ripple forms preserved on a sandstone bedding surface; small desiccation cracks and bioturbation are also evident; isolated channel-fill (ICF) element, Organ Rock Formation; O) ICF element preserved between underlying and overlying Adu units, Cedar Mesa Sandstone; rucksack for scale; P) dark purple-brown multilateral- and multi-storey amalgamated channel (ACF) elements interbedded between orange aeolian dune units (Adu), Undivided Cutler Group; observed cliff section is 50 m high; Q) dark purple-brown amalgamated channel (ACF) element with erosive base, Undivided Cutler Group; observed cliff section is 30 m high; R) fluvial cross-bedded sets, some with extraformational pebbles, others with soft-sediment deformation structures, lower Cutler beds; S) fluvial sheet-like (SFD) element bounded by underlying and overlying Adu units, Cedar Mesa Sandstone; T) vertically stacked fluvial sheet-like (SFD) elements (dark orange); a prominent beige-colour aeolian dune sequence (Adu) is present in the centre of the cliff section; aeolian reworked fluvial deposits (probably of loess origin) are preserved as FLR elements (light orange); Organ Rock Formation; observed cliff section is ~150 m high; U) and V) two examples of trench-like fluvial incisions into underlying Adu units; the bases of the channel fills contain reworked aeolian blocks (indicated by arrows); these are DR elements, Organ Rock Formation; rucksack for scale in U; observed cliff section is 20 m high in V; W) sandstone intraclasts of aeolian origin (Fhc facies) preserved in fluvial deposits of a DR element, Organ Rock Formation; X) aeolian reworking of sediments that were likely originally of fluvial origin (FLR element), lower Cutler beds.*

## 4. Results: preserved sedimentary record of aeolian-fluvial interaction

Here, we describe the sedimentology of 8 distinct but commonly occurring types of aeolian-fluvial interaction identified in the Permian deposits of the Cutler Group (Table 3; Figure 3). These 8 types are defined and characterized through analysis of 521 architectural elements depicted in 24 architectural element panels. The preserved sedimentary record of aeolian-fluvial interactions described here is also recognized in many other ancient sedimentary successions of aeolian-fluvial origin of different ages and from different geographic locations. The significance of these results in terms of interpretation of processes and controls on the aeolian-fluvial sedimentological record is considered in following Discussion.

***FIGURE 4 (2-column fitting).*** *Schematic architectural panels depicting the range of different sedimentary units, elements and geometries typical of preserved water-table-controlled interdune elements (Langford & Chan, 1989; Crabaugh & Kocurek, 1993; Mountney & Jagger, 2004). Key features and idealized successions are shown. In addition to example architectures from the Permian Cutler Group, an example from the Jurassic Navajo Sandstone in southeast Utah is also shown.*

***FIGURE 5 (2-column fitting).*** *Schematic architectural panels depicting the range of different sedimentary units, elements and geometries typical of interdune restricted low-energy deposition*

*originating from flood input (Langford & Chan, 1989; Mountney, 2006b). Key features and idealized successions are shown.*

***FIGURE 6 (2-column fitting).*** *Schematic architectural panels depicting the range of different sedimentary units, elements and geometries typical of episodic fluvial deposition originating from confined flooding in interdune corridors parallel to the dune crest-line trend (Langford & Chan, 1989; Herries, 1993). Key features and idealized successions are shown.*

***FIGURE 7 (2-column fitting).*** *Schematic architectural panels depicting the range of different sedimentary units, elements and geometries typical of episodic fluvial deposition originating from confined flooding in interdune corridors perpendicular to the dune crest-line trend (Langford & Chan, 1989; Herries, 1993). Key features and idealized successions are shown.*

***FIGURE 8 (2-column fitting).*** *Schematic architectural panel depicting the range of different sedimentary units, elements and geometries typical of long-lived floods confined within interdune corridors (Langford & Chan, 1988, 1989; Herries, 1993; Carr-Crabaugh & Kocurek, 1998; Mountney & Jagger, 2004). Key features and idealized successions are shown. Diagram depicting bypass supersurface generation modified in part from Langford & Chan (1988).*

***FIGURE 9 (2-column fitting).*** *Schematic architectural panels depicting the range of different sedimentary units, elements and geometries typical of unchannelized fluvial deposition in outer-erg settings (Mountney & Jagger, 2004; Cain & Mountney, 2011). Key features and idealized successions are shown.*

***FIGURE 10 (2-column fitting).*** *Schematic architectural panel depicting the range of different sedimentary units, elements and geometries symptomatic of catastrophic flooding in dune field (Ahmed Benan & Kocurek, 2000; Svendsen et al., 2003; Cain & Mountney, 2011; Ferronatto et al., 2019). Key features and idealized successions are shown.*

***FIGURE 11 (2-column fitting).*** *Schematic architectural panel depicting the range of different sedimentary units, elements and geometries symptomatic of fluvial deposits reworked by aeolian processes (Simpson et al., 2008; Cain & Mountney, 2011). Key features and idealized successions are shown.*

### *4.1. Water-table-controlled interdune elements*

Of the 521 architectural elements examined, 149 are of this type (29%). Ancient aeolian successions demonstrating influence by fluctuating water-table levels are characterized by thin deposits (mean observed dimensions are ~1 m thick and 85 m wide; maximum observed dimensions are ~5 m thick

and up to at least 354 m wide [unconstrained]) of clay to very fine-grain sand (Fig. 4). These are wet (*WID*) and damp (*DID*) interdune elements. They occur mostly as lens-shaped bodies of red silty sandstone (*Awit*; *Adit*) between aeolian dune deposits (*Adu*) (Langford & Chan, 1989; Mountney & Thompson, 2002; Mountney & Jagger, 2004; cf. Priddy & Clarke, 2020) (Fig. 3B-I). Only rarely do the lenses exhibit erosive bases (5% and <1% of cases oriented perpendicular and parallel to aeolian dune migration, respectively). Rarely, interfingering and gradual transition between neighbouring aeolian dune deposits (*Adu*) and interdune elements is observed. The geometry of examples of this type of architectural element is commonly similar, regardless of the orientation in which it is viewed: elements that occur in cross-sections oriented parallel to the aeolian palaeo-transport direction (57%) are of only marginally greater lateral extent than those oriented perpendicular to palaeo-transport direction (43%); mean lateral extents in these orientations are 90 m and 85 m, respectively.

Two common facies associations make up the fill of wet (*WID*) and damp (*DID*) interdune elements (Table 3). Facies Association 1 (FA1), which is typical of *WID* elements, is characterized dominantly by planar laminated claystone and siltstone (mudstone), chert (silcrete) beds, rare fine sandstone beds, burrows, bedding-surface crawling trace fossils of invertebrates, evaporitic minerals such as halite and gypsum, and soft-sediment deformation structures in the form of contorted bedding. Desiccation cracks are not uncommon. Facies Association 2 (FA2), which is typical of *DID* elements, is characterized by siltstone and very-fine sandstone, wavy lamination, adhesion warts and ripples (and their stratification), desiccation cracks, calcrete nodules (in some cases in layers), rhizoliths, burrows and raindrop impact marks on bedding surfaces. Both of these facies associations may be capped or interbedded with palaeosols (*Pls*) or freshwater limestones (*Clc*). The majority of *WID* and *DID* architectural elements (74%) are expressed as lenticular units that occur directly beneath the basal-most parts of aeolian trough cross-bedded sets; other recorded examples of these elements (26%) are laterally continuous over distances greater than the widths of large aeolian trough cross-bedded sets of overlying aeolian dune elements.

### *4.2. Low-energy deposits originating from fluvial flood input*

Here we describe the architecture of interdune elements associated with low-energy and mostly non-destructive (i.e., passive) and non-channelized fluvial flooding. Herein, the term “flood” refers to flowing surface water of meteoric, fluvial or groundwater origin, without reference to scale. Processes associated with fluvial flooding may occur in combination with groundwater fluctuation (Section 3.1).

Of the 521 architectural elements examined in total, 154 are of this type (30%). Deposits of low-energy floods (*LED*) in aeolian dune-field (erg) successions are characterized by thin but laterally extensive elements (mean observed dimensions are 1.5 m thick and 125 m wide; maximum observed dimensions are 18 m thick and 700 m wide) of silt to very fine-grain sand interleaved with aeolian dune units (*Adu*) (Fig. 3J-K; Fig. 5). These elements occur most commonly as lens-shaped bodies preserved directly beneath the bases of trough-shaped, cross-stratified aeolian dune units. Elements observed in cross-sections oriented parallel to the aeolian palaeo-transport direction (49% of examples) have a mean width of 114 m; elements observed oriented parallel to the aeolian palaeo-transport direction (35% of examples) have a mean width of 138 m; other examples are oblique to these orientations. The majority of these elements exhibit sharp but non-erosive bases. However,

small channel scours (<0.5 m incision) are present in 15% of elements of this type and these are observed in orientations both perpendicular and parallel to aeolian dune migration.

Internally, *LED* elements are composed of Facies Association 3 (FA3), which is characterized by siltstone to very fine sandstone, minor channel scours, asymmetrical current ripple forms on bedding surfaces and current-ripple lamination indicative of unidirectional currents, bidirectional (oscillatory) current ripple forms and stratification, small plant root traces (rhizoliths), bioturbation and trace fossils (burrows) (Table 3). Units of this facies associations may be capped or interbedded with thin calcrete palaeosols (*Pls*) and/or thin beds of freshwater limestones (*Clc*).

### *4.3 Isolated ribbon-shaped channel-fills originating from episodic confined flooding of interdunes in orientations parallel to the trend of dune crestlines*

Of the 521 architectural elements examined in total, 46 are of this type (9%). Architectural elements associated with episodic, confined fluvial flooding of interdunes in orientations parallel to the trend of dune crestlines (*ICF*) are characterized by ribbon-shaped bodies dominantly of fine sandstone (*Fedr*) (Fig. 3L-O). Rare conglomerates in the form of pebble lags may be present directly above basal bounding surfaces (Fig. 6). In cross-sections oriented parallel to aeolian palaeo-transport, these elements are apparently lens-shaped (mean observed dimensions are 1 m thick and 40 m wide; maximum observed dimensions are 3 m thick and 120 m wide). In 85% of examples of *ICF* elements, basal-most bounding surfaces are erosive such that they define channels that incise downward and erode into underlying aeolian dune units (*Adu*); locally, incision is 2 to 4 m deep. However, in cross-sections perpendicular to aeolian palaeo-transport, these elements can be traced continuously along their length for distances of several thousand metres, in some cases. Thus, these isolated elements exhibit a ribbon-like geometry.

These architectural elements are characterized internally by Facies Association 4 (FA4), which is composed dominantly of the occurrence of sets and cosets of cross-bedded fluvial sandstone (bedforms and barforms); the azimuths of preserved forests in these cross-stratified sets record fluvial palaeocurrent directions that differ markedly (up to 90 degrees) from aeolian dune foreset azimuths; this is a key defining characteristic to demonstrate paleoflow that was parallel to the trend of the crestlines of neighbouring aeolian dunes (Table 3). Facies Association 4 may additionally comprise beds of pebbly sandstone or conglomerate (with either intraformational or extraformational pebble clasts). Associated sedimentary structures and features include lower flow-regime planar laminations of aqueous origin (*Flp*), burrows, rhizoliths and capping units of calcretes (*Clc*) and palaeosols (*Pls*). Vertical transitions from *ICF* elements to overlying low-energy fluvial deposits (*LED*) of FA3 (Section 3.2) are common.

### *4.4. Isolated ribbon-shaped channel-fills originating from episodic confined flooding of interdunes in orientations perpendicular to the trend of dune crest-lines*

Of the 521 architectural elements examined in total, 75 are of this type (14%). Architectural elements associated with episodic, confined fluvial flooding of interdunes (*ICF*) may also develop in orientations perpendicular to the trend of dune crestlines; they are characterized by lenticular bodies

dominantly of fine-grain sand (*Fedr*) with rare occurrence of basal conglomerate in the form of pebble lags directly above basal bounding surfaces (Fig. 3L-O; Fig. 7). In cross-sections perpendicular to aeolian palaeo-transport, elements are ca. 1.3 m thick and ca. 65 m wide (maximum 4.8 m thick and 325 m wide). The bases of these elements are erosive: channel-fills incise downward and erode into underlying units with up to 6 m of local incision evident: ca. 90% of elements of this type have erosive bases. In cross-section oriented parallel to the reconstructed direction aeolian transport, elements are laterally highly extensive (several km, in some cases) and continuous, and show only limited relief on basal incision surfaces. Lenticular channel-shaped geometries are mainly evident in panels oriented perpendicular to aeolian palaeo-transport direction.

Channel-fills comprise Facies Association 4 (see Section 3.3 above). The azimuths of preserved forests in these cross-stratified sets record fluvial palaeocurrent directions that are similar to aeolian dune foreset azimuths present in adjoining aeolian dune deposits; this is a key defining characteristic to demonstrate paleoflow that was perpendicular to the trend of the crestlines of neighbouring aeolian dunes. The enclosing aeolian units are composed of both aeolian-dune facies (*Adu*) and plane-bedded aeolian sand-sheet facies (*Assh*) characterized by well-sorted aeolian wind-ripple strata and aeolian plane-bed strata. Vertical transitions from channel-fill deposits (FA4) to overlying aeolian sand-sheet deposits commonly preserve interbedding of the two types.

### *4.5. Amalgamated channel-forms resulting from long-lived confined flooding*

Of the 521 architectural elements examined in total, 63 are of this type (12%). Aeolian dune-field systems affected by long-lasting and repeated confined flood events are characterized by fine to medium sandstone fluvial deposits (*Fldr*) with common pebble lags (Fig. 8). Architectural elements are represented by sheet-like units of amalgamated channel-forms (*ACF*) of considerable lateral extent and thickness (mean observed dimensions are 3.5 m thick and 262 m wide; maximum observed dimensions are 9.5 m thick and 318 m wide) (Fig. 3P-Q). Channel fills are commonly preserved as a single-storey sandstone body, though multistorey bodies (2 or 3 vertically stacked channel-fill storeys) are also recorded in places. Channel fills occur laterally juxtaposed to form multilateral channel belts. These *ACF* channel-belt elements occur intercalated between aeolian dune units (*Adu*). The bases of these elements exhibit marked incision: ca. 70 % of elements have erosional bases with up to 3 m of relief.

The fill of these elements comprises Facies Association 5 (FA5), which is defined by the occurrence of numerous fluvial cross-bedded and plane-bedded sandstone sets and cosets, climbing ripple strata, calcrete nodules (in some cases forming layers), rhizoliths and burrows. Lateral facies variations to finer sandstone are common. Localized occurrences of bioturbation, rhizoliths, and bleaching and mottling are associated with some large examples of this type of element (Table 3).

The lateral continuity and extent of these elements is similar in orientations both parallel and perpendicular to aeolian transport (only ca. 8 m difference in average width in examples from the two cross-section orientations); this demonstrates the extensive, sheet-like geometry of the bodies. Two major architectural relationships are evident at the boundaries between sheet-like channel belts (*ACF*) and enclosing aeolian units (*Adu*): (i) in small number of instances, intertonguing geometries are

recorded where channel wings pinch out against aeolian sandstones; (ii) in the majority of instances, major amalgamated channel units (formed of laterally juxtaposed *ACF* elements) are laterally highly continuous and record no evidence of fluvial and aeolian intertonguing. Prior studies of examples of the latter variety of this element have noted their region-wide extent and continuity: up to 400 $km^2$. This type of element therefore serves as a useful regional marker for stratigraphical correlation (Langford & Chan, 1989). This latter variety is an especially common aeolian-fluvial interaction type in the Organ Rock Formation (Cain, 2009). It is also common in the lateral outer erg-margin region of the Cedar Mesa Sandstone (Langford and Chan, 1988; 1989; Mountney and Jagger, 2004).

### *4.6. Unconfined sheet-like flood deposition*

Of the 521 architectural elements examined in total, 25 are of this type (5%). Architectural elements associated with non-channelized, unconfined flooding of interdune areas (*SFD*) are defined by thick and laterally extensive elements (mean thickness is 2.5 m; maximum thickness of 7.5 m) of fine to medium-grain fluvial sandstones (*Fsh*). These sandstone deposits may onlap the preserved flanks of adjoining aeolian dune units (*Adu*) but only 12% of examples demonstrate evidence of erosion at the contact. These *SFD* architectural elements are characterized by great lateral extent: all recorded examples of this element exceed the lateral limits of the outcrops studied (Fig. 3S-T). Therefore, their true width is unconstrained but is at least 2,000 m (Fig. 9). They have apparently similar dimensions in all orientations.

The fill of *SFD* elements comprises Facies Association 6 (FA6), which is characterized by fine- to medium-grain sandstone with primary current lineation indicative of upper-flow regime conditions (Table 3). Siltstone to very fine-grain sandstone is also common and may occur interlaminated or interbedded. Rhizoliths are common. Palaeosols (*Pls*) with lens-like geometries are recorded, but are not common. Rare aeolian dune deposits (*Adu*) may occur preserved entirely encased within fluvial deposits of FA6.

### *4.7. Fluvial breaching of dunes and their reworking by catastrophic flooding*

Of the 521 architectural elements examined in total, 9 are of this type (1.7%). Ancient erg-margin systems affected by catastrophic fluvial flooding and corresponding aeolian dune (*Adu*) reworking are associated with thick fluvial deposits (mean thickness is 4.2 m), some of which are notably laterally extensive and continuous (mean width is 265 m). One large instance of an architectural element of this type has a maximum thickness of 7 m and a lateral extent of 445 m. These architectural elements (*DR*) directly overlie and incise downward into aeolian dune units (Table 3; Fig. 3U-W; Fig. 10).

Internally, deposits of *DR* elements constitute Facies Association 7 (FA7): (i) erosional base with marked high-relief incision (several metres); (ii) in some cases, a lower fill of coarse- to very coarse-grain, moderately to poorly sorted sandstone, some with pebble to boulder intraformational clasts (blocks) of aeolian sandstone; (iii) in all cases, a fill of very fine- to medium-grain, well-sorted sandstone, commonly with climbing current-ripple lamination and/or normally graded structureless units, some with intraformational mud-chips as floating clasts (cf. Svendsen et al., 2003). Locally,

marked erosive relief at the base of *DF* elements is expressed as trench-like cuts with near-vertical or concave sides (cf. Ferronatto et al., 2019) that incise into underlying aeolian dune units. The fill of these erosive cuts commonly contains especially large (decimetre-diameter) intraformational rip-up clasts of aeolian reworked sandstone present as blocks in the lowermost deposits (cf. Ellis, 1993; Cain & Mountney, 2011). Such blocks may internally preserve relic aeolian dune cross bedding.

### *4.8. Aeolian reworking of fluvial deposits*

This type of interaction is common in modern arid environments but is only rarely identified in ancient preserved sedimentary successions. Detailed analyses of relic fluvial barform topographies reveals thin layers of fine-grain sandstone that is better-sorted than the deposits of the fluvial sandstone elements that they mantle (Fig. 3X). In places, pinstripe wind-ripple lamination (*Afl*) is evident in the better-sorted deposits (Fig. 11). Elsewhere, architectural elements (*FLR*) with steep incised margins and channel-shaped geometries indicative of erosion are evident, but their fill is entirely of cross-bedded aeolian dune sandstone (*Adu*). In similar instances, the base of the channel fill may be of fluvial sandstone (e.g., *Fedr*), but the upper part of the channel fill is of cross-bedded aeolian dune sandstone (*Adu*). In some cases, the channel forms are preserved between major aeolian dune units; in such cases, they incise down into the underlying aeolian dune unit and are overlain by a sharp surface defining the base of the overlying dune unit.

## 5. Discussion

A sedimentologically diverse but commonly occurring set of architectural elements in preserved successions that form a record of competing aeolian-fluvial depositional systems has been identified. Qualitative and quantitative characterization of 521 architectural element geometries has been undertaken based on assessment of cross-sections that are variably oriented in relation to the direction of aeolian palaeo-transport and to the reconstructed trend of aeolian dune crestlines. The generalized architectural panels (Figs. 4-11) are representative of each interaction type; they depict typical geometries and relationships. Here, we discuss the palaeoenvironmental significance of the preserved sedimentary record of aeolian-fluvial interaction. The 8 distinct types of interaction form the basis for a novel and generally applicable classification scheme (Fig. 12).

***FIGURE 12 (2-column fitting).*** *Summary of the range of architectural element dimensions, geometries, boundary types, and diversity of sedimentary features observed in examples of the preserved sedimentary expression of aeolian-fluvial interaction in the Cutler Group. Some primary data used to construct this figure are in part from Jagger (2003), Cain (2009) and Wakefield (2011). Given the generally small scale of observation scale of FLR elements – centimetre to decimetre – no data are recorded in this figure for interaction type 8.*

### *5.1. Water-table-controlled interdune elements*

Deposits of Facies Association 1 (FA1), with diagnostic planar laminated claystone and siltstone (mudstone) beds and associated features (Table 3), are attributed to episodic events whereby the water-table rose above the level of the interdune floor (Mountney & Jagger, 2004); these are wet interdune elements (*WID*) (Fig. 3B-D). Deposits of Facies Association 2 (FA2), with wavy

laminations, adhesion structures and raindrop impact marks, are attributed to the deposition of windblown sand over a damp surface to generate adhesion structures on the floor of an interdune dampened by the capillary fringe of a water-table that lay below but nevertheless close to the surface; these are damp interdune elements (*DID*) (cf. Mountney, 2006a) (Fig. 3E-I).

In wet aeolian systems (*sensu* Kocurek & Havholm, 1993), accumulation is controlled by the level of the groundwater (Carr-Crabaugh & Kocurek, 1998); the architectures of wet and damp interdune elements are governed in part by the angle of climb of dunes that were contemporaneously active alongside the interdunes in the system. The maintenance of wet or damp interdune surface conditions determines the manner by which the wet or damp interdune units will accumulate and how the facies association and succession that results from that accumulation will be preserved (Fig. 4). Some interdune elements may transition laterally from wet to damp, dependent on how the water-table interacted with the accumulation surface in the original interdune pond and at its fringe (Mountney & Jagger, 2004; cf. Driese, 1985).

Factors that control the preserved architecture of interdune pond elements are as follows: (i) the spacing of the original dunes that bound the interdune; (ii) the original interdune dimensions (width and length relative to the trends of neighbouring aeolian dune crestlines); (iii) the plan-view variability of the shape of the interdunes as determined by the presence or absence of neighbouring dunes with straight or curved (in some cases sinuous) crestlines; and (iv) the availability of sediment to be accumulated as the interdune deposit; (v) the rate of original interdune advance (migration) between mobile neighbouring dunes; (vi) changes in the shape and size of the interdune over time; (vii) the longevity (lifespan) of the interdune (cf. Mountney, 2012).

In accumulating aeolian systems, the trajectory of climb is determined by an evolving rate according to variations in one or more of the above-mentioned factors (Crabaugh & Kocurek, 1993; Mountney, 2012). In cases where the rate at which the dune and adjoining interdune advance (migration) markedly exceeded the rate of relative water-table rise, a low angle of climb results; system climb to generate architectural elements in the accumulated stratigraphy is low such that it cannot typically be observed at the scale of an individual damp or wet interdune element. An interdune migration bounding surface is defined at the base of both dam and wet interdune elements (Fig. 2). Both this surface and the deposits of the associated overlying element appear apparently close to palaeo-horizontal at the scale of an individual outcrop (Mountney, 2006; Wakefield & Mountney, 2013).

Where aeolian dune units occur interleaved between wet and damp interdune elements in a manner that demonstrates interfingering of dune and interdune deposits, evidence is preserved to demonstrate the co-migration (and potentially the concomitant “climb”) of both the interdune element and the adjoining dune elements. Interfingering, sometimes referred to as intertonguing or feathering, between aeolian units and interdune elements (dune lee-slope slipface deposits merging into interdune deposits) is an important relationship to demonstrate synchronous deposition (Pulvertaft, 1985; Mountney & Thompson, 2002).

Rare instances of scour at the bases of some wet interdune elements are attributed to flood incursion along the original interdune corridor, possibly where flood waters converged in response to runoff during and immediately following intra-dune-field rainfall.

Lateral and vertical facies changes from the wet to the damp interdune facies associations are a type of drying-up cycle (cf. Mountney et al., 1998; Mountney & Thompson, 2002). The association of damp and wet interdune elements with directly overlying palaeosols (*Pls*) indicates stabilization and soil development. Long-lasting damp or wet surface conditions result in soil and vegetation development at the shoreline fringes of shallow interdune ponds. The association of damp and wet interdune facies associations with overlying freshwater limestone deposits (*Clc*) indicates a water-table that lay above the accumulation surface for a protracted period, but for which there was little clastic sediment input (cf. Driese, 1985; Mountney & Jagger, 2004). If high water-table levels are followed by drought conditions, evaporitic carbonate deposition can result, as for the fringes of playa-lakes (e.g., Herries, 1993; Herries & Cowan, 1997). Soft-sediment deformation, such as contorted strata or collapse features, can occur during the time on onset of sediment compaction or early lithification in cases where the sediments are water saturated (Owen et al., 2011; Suter et al., 2011).

### *5.2. Low-energy deposits originating from fluvial flood input*

Deposits of Facies Association 3 (FA3) are the product of low-energy (i.e., passive) flooding of interdune corridors and hollows (Fig. 3J-K; Fig. 5), in some cases likely close to the point of termination of a fluvial incursion (cf. Al-Masrahy & Mountney, 2015). These low-energy flood deposits record (i) settling of suspended-load when the water discharge is too low to perpetuate directed flow in the interdune setting, (ii) waning flow that remained sufficient to enable aqueous bedform migration and deposition (current ripples and current-ripple stratification are important diagnostic criteria), and (iii) interdune ponds with wave activity due to wind shear on the water surface (oscillatory ripples) (Kocurek, 1981). The aqueous flows passing along these interdune corridors were mostly non-channelized and non-erosional: as such they are mostly a type of overbank flow (*Flp*), albeit within the confines of an interdune (Langford & Chan, 1989). Despite a higher portion of scour features than in wet (*WID*) and damp interdune elements (*DID*), low-energy fluvially flooded interdune elements (*LED*) only record evidence of minor incision and erosion (Fig. 12). Soil development (*Pls*) may be promoted by this type of overbank deposition (Demko et al., 2004). In the case of a dune-dammed flood incursion, the resulting body of ponded water may slowly infiltrate or evaporate (Stanistreet & Stollhofen, 2002), thereby accumulating mudstone or evaporitic limestone (*Clc*) deposits. Aqueous current and/or oscillation ripples and ripple stratification are key discriminatory features to differentiate low-energy fluvially flooded interdune elements (*LED*) from wet (*WID*) and damp interdune elements (*DID*) (Table 3).

The termination of fluvial flood incursions by dune damming is especially common in dune-field margin settings (e.g., Krapf et al., 2003; Svendsen et al., 2003), but can also occur in the more central parts of dune fields, either where extrageneous fluvial systems have been able to penetrate long distances along open interdune corridors (Al-Masrahy & Mountney, 2015), else in response to the capture and ponding of locally derived surface run-off in transient enclosed interdune ephemeral lakes (Mountney, 2006b); in the latter case, deposits tend to be of fine sand.

The architecture of low-energy fluvially flooded interdune elements is governed by the following: (i) intensity of the fluvial floods; (ii) the repeat frequency of flood events; (iii) the rate of migration of interdune hollows and/or corridors developed between migrating aeolian dunes; (iv) the accumulation of the overall aeolian dune-field system expressed by the angle of climb of the system.

### *5.3 Isolated ribbon-shaped channel-fills originating from episodic confined flooding of interdunes in orientations parallel to the trend of dune crestlines*

Deposits of Facies Association 4 (FA4), with prominent channel-scours, and fluvial bedform and barform deposits, are attributed to channelized fluvial incursion. In some cases this takes place along laterally extensive open interdune corridors by ephemeral fluvial streams in orientations approximately parallel to the trend of dune crestlines (Fig. 6), as demonstrated by a marked difference in palaeocurrent indicators of fluvial versus neighbouring aeolian dune facies units (commonly a right angles) (cf. Herries, 1993; Al-Masrahy & Mountney, 2015); these are isolated ribbon-shaped channel-fill elements (*ICF*) (Fig. 3L-O). Isolated channel-fill elements record flow in wadi-type channels with marked incisional bases (Fig. 12). Channels extend along interdune corridors between confining linear or transverse aeolian dunes. The confinement of a fluvial channel within a narrow interdune corridor concentrates flood waters, thereby increasing stream power and promoting channel incision (Al-Masrahy & Mountney, 2015). The common upward facies transition to finer depsits of fluvial origin records a temporal decrease in the energy of the flow regime as floods waned, else the transition to overbank deposition (*LED*). The ribbon-shape of *ICF* elements suggests that the fluvial flood events responsible for their generation were relatively short-lived: successive floods were unlikely to repeatedly reoccupy the same interdune corridor as it gradually translated in front of migrating aeolian dunes (cf. Langford and Chan, 1989; Herries, 1993).

### *5.4. Isolated ribbon-shaped channel-fills originating from episodic confined flooding of interdunes in orientations perpendicular to the trend of dune crest-lines*

Deposits of Facies Association 4 are attributed to channelized fluvial flooding of the interdune areas by ephemeral fluvial incursions; this generates isolated ribbon-shaped channel-fill elements (*ICF*) (Fig. 3L-O). However, this element differs from the equivalent element described and interpreted in Sections 3.3 and 4.3 because it records evidence of fluvial incursion oriented perpendicular to the trend of dune crest-lines, as revealed by the vector mean orientation of cross-bedded sets of both fluvial and aeolian origin, which record either similar or directly opposing bedform migration directions) (Fig. 7). Aeolian sand-sheet facies (*Assh*) with characteristic beds of wind-ripple strata are attributed to the deposition of windblown sediments on a low-relief surface. The elements described here record episodic, confined fluvial flooding of interdunes but for which the isolated channel-fill elements do not follow a path created by elongate interdune corridors (cf. Al-Masrahy & Mountney, 2015). Rather, the fluvial channels flowed between and around aeolian dunes. This type of aeolian-fluvial interaction is only possible where dunes do not form elongate (i.e., laterally extensive) and continuous topographic ridges. Such aeolian system characteristics are common in outer-erg margins where aeolian sand-sheets are the dominant geomorphic setting. In some inner-erg margin settings, where aeolian dunes are more numerous, breaks in dune ridges might allow fluvial channels to pass across to neighbouring interdune corridors. Channelized floods may breach relatively low-relief dune ridges by incising aeolian deposits, for example at a low-lying col (see Section 5.7).

The prevalence of aeolian sand-sheet deposits in the accumulated succession indicates a system for which sediment is supply-limited or availability-limited (*sensu* Kocurek & Lancaster, 1999) and within which aeolian dunes are spatially disconnected, thereby enabling channelized ephemeral streams to flow in a path normal to the general trend of dune crestlines. The common association of ribbon-channel *ICF* elements and aeolian sandsheet (*Assh)* facies units, together with the relative orientation of palaeocurrent indicators (e.g., cross bedded foresets) in ribbon-shaped channel-fills of *ICF* elements and adjoining aeolian dune units (*Adu*) are the key diagnostic criteria with which differentiate *ICF* elements oriented perpendicular to the trend of aeolian dune crestlines (Section 5.4) from their counterparts oriented parallel to the trend of aeolian dune crestlines (Section 5.3) (Table 3).

### *5.5. Amalgamated channel-forms resulting from long-lasting confined flooding*

Deposits of Facies Association 5 (FA5), with diagnostic continuous units of highly erosive-based channel-forms, and fluvial barforms with cross-bedded sets and aqueous climbing-ripple strata (Fig. 12), correspond to the preserved strata of long-lived, repeated, yet confined flooding events within interdune areas (Langford & Chan, 1988, 1989; Herries, 1993). Repeated flood events generate amalgamated sheet-like elements composed of multilateral and, in some cases, multistorey fluvial channels (*ACF*) (Fig. 3P-Q; Fig. 8). Neighbouring elements of finer material, with rhizoliths and burrows are attributed to associated floodplain and overbank deposits (*LED*).

Unlike isolated ribbon-shaped channel-fill elements *(ICF*), long-lived fluvial incursions generate sheet-like elements by repeatedly flooding along interdune corridors, which themselves move laterally over time between migrating aeolian dunes. Thus, as an interdune corridor migrates, so the floods which pass along that corridor are translated over time. Flood deposits thereby build a sheet-like architecture over multiple flood events. The geometry of sheet-like *ACF* elements is controlled by (i) the rate of lateral translation of the interdune corridor, (ii) the frequency of flooding events (Stanistreet & Stollhofen, 2002), and (iii) the angle of climb of an accumulating system, which may vary from zero (i.e. bypass) to a low but positive value (i.e. climbing).

For aeolian systems that accumulate via bedform climb, the angle of climb is typically not constant and may not always be positive. Fluvial incursions may act to limit the availability of sediment supply suitable for aeolian dune construction. As such, the overall system may undertake episodes of bypass (i.e., zero angle of climb). Aeolian dunes may persist but will only translate horizontally. Fluvial channels emplaced along interdune corridors will build laterally over successive flood events as the aeolian dune and interdune gradually migrate laterally (Langford & Chan, 1988, 1989). If the frequency of flooding is high relative to the rate of lateral migration, a continuous sheet-like fluvial element of multilateral channel bodies will accumulate. A bypass supersurface (a flood surface in the terminology of Langford & Chan, 1988, 1989) will define the base of the sheet-like *ASF* element. These elements are documented from variety of aeolian-fluvial systems (Carr-Crabaugh & Kocurek, 1998; Mountney & Jagger, 2004; Mountney, 2012). If the frequency of flooding is low relative to the rate of lateral migration, fluvial flood deposits might be expressed as isolated ribbon (*ICF*) elements, possibly with multiple instances at a similar stratigraphic level.

The development of amalgamated sheet-like multilateral channel-belt elements (*ACF*) may be indicative of a shift toward increased fluvial influence in the depositional system, possibly driven by a change to more humid climate conditions (Veiga et al., 2002; Jordan & Mountney, 2010; Spalletti et al., 2010).

### *5.6. Unconfined sheet-like flood deposition*

Deposits of Facies Association 6 (FA6), with conformable bases (Fig. 12) and beds of primary current lamination, are attributed to unconfined flooding of the interdune area; these are sheet-like flood deposits (*SFD*) (Mountney & Jagger, 2004; Cain & Mountney, 2011) (Fig. 3S-T). Such non-channelized flows are mainly distinguished from floodplain and overbank elements (*LED*) by the overall coarser grain size of the deposits and the predominance of sedimentary structures indicative of upper-flow regime sedimentation (Fig. 9). These *SFD* elements may be generated by heavy rainfall events in outer-erg settings, especially near mountain-range catchments, where floods rise toward peak discharge rapidly such that flowing water cannot be confined within a channel. The proximity of eroding catchments explains the coarser sediment sizes. Such deposits could be the preserved deposits of fluvial incursions that emanated from a single point source into a dune field, else from multiple point sources, or line sources (cf. Al-Masrahy & Mountney, 2015). Lenses of siltstone and very-fine sandstone may represent falling-stage deposits, else may be attributed to Facies Association 3 (*LED*).

### *5.7. Fluvial breaching of dunes and their reworking by catastrophic flooding*

Deposits of Facies Association 7 (FA7) with diagnostic (i) erosive basal surfaces forming trench-like channel cuts, (ii) intraformational rip-up clasts, and (iii) mud-chip floating clasts were likely deposited from hyper-concentrated flows (*Fhc*) and intra-erg mass flows (*Fmf*). Deposits of *DR* elements are fluvially reworked aeolian dune sand (Fig. 3U-W; Fig. 10). Hyper-concentrated flows can cause local inundation and drowning of the dune field (Svendsen et al., 2003; Cain & Mountney, 2011). If dunes are partly consolidated, trench-like channels can be carved out by the catastrophic flood events, and weakly indurated (or cemented) debris of aeolian deposits may be locally eroded and reworked as blocks. Such blocks might be the product of slumping of dune slopes (Loope et al., 1999). Despite initially being highly erosive during the rise to peak discharge, later waning flows (intra-erg mass flows) tend to be non-erosive, despite their high energy; their deposits may pond upstream of remnant aeolian dune topography and may drape it (Ahmed Benan & Kocurek, 2000; Svendsen et al., 2003). Processes causing these two types of deposition are distinguished by the density and rheology of the fluid, and thus by flow regime: hyper-concentrated flows are characterized by turbulent flows; intra-erg mass flows are a type of laminar flow with no appreciable erosive capacity (Svendsen et al., 2003). Toward at the end of the flood event, a reduction in flood energy promotes the rapid development of aqueous bedforms; notably rapid reduction in energy can enable the accumulation of structureless sand deposits, in some cases with “floating” clasts of finer material.

### *5.8. Aeolian reworking of fluvial deposits*

The mantling of fluvial bed-sets by fine-grain, well-sorted coarse silt and sand deposits, comonly with wind-ripple strata, indicates the partial deflation of fluvial barforms and re-working of deposits

by aeolian processes, likely during drier episodes when the tops of fluvial bars dried out (Simpson et al., 2008; Cain & Mountney, 2011) (Fig 3X). The occurrence of steep-sided, incised channels filled mostly or entirely with aeolian dune deposits (Fig. 11) demonstrates an episode of fluvial incision but where the channel is left wholly or largely unfilled by fluvial deposits. Thus, a local accommodation hollow is available to be filled by a later migrating aeolian dune: aeolian sediments may fill the topographic hollow, thereby preserving the ancient erosive contact with the underlying aeolian unit. These are wind-reworked fluvial deposits (*FLR*).

### *5.9. Significance and application*

The generalized classification scheme for the preserved sedimentary expression of common types of aeolian-fluvial interaction presented here is significant because it assists in our interpretation of the record of palaeoenvironment change in the geological record. Architectural-element geometries vary depending on a series of controls: (i) the length of time over which the substrate conditions (dry, damp, wet) are maintained in an interdune; (ii) the size of the interdune, and notably its extent such that it might maintain an open corridor along which fluvial systems might pass during flood incursions into the aeolian dune field; (iii) the rate of lateral translation of the interdune developed between migrating aeolian dunes; (iv) the rate of vertical accumulation of the succession. Of these the ratio between the rate of lateral translation and the rate of vertical accumulation define the angle of climb of the system (Mountney, 2012). Together, variations in these parameters can interact to generate spatial and temporal variability in the preservation of aeolian-fluvial interactions of different types. The classification scheme proposed here provides a way to assess the palaeoenvironmental significance of commonly observed types of aeolian-fluvial interaction, and to link those to their modern geomorphic equivalents (Fig. 13). In addition to gaining a good understanding of the general palaeoenvironmental characteristics of a studied section, it is important while applying this type of classification scheme to consider in as much detail as possible the outcrop orientations from which architectural elements are observed. Conclusions about aeolian-fluvial interaction styles should be drawn with prudence when working with data sets for which three-dimensional architectural relationships cannot be established with confidence.

***FIGURE 13 (2-column fitting).*** *Integrated dynamic facies model for a fluvial-influenced aeolian erg margin displaying different interaction styles between aeolian and fluvial depositional systems with temporal and spatial variations as a consequence of changes in geomorphic controls. Hills, aeolian topographies and fluvial channels are not depicted to scale.*

The model for sedimentary accumulation and preservation on which this classification is constructed accounts primarily for translation and climb of aeolian bedforms. However, alternative interdune aggradation models have been proposed in the past, including for parts of the Cedar Mesa Sandstone of the Cutler Group (Langford et al., 2008). On a local scale, aeolian topography can influence sediment accumulation during dune-stabilization stages through the filling of interdune hollows by aeolian sand-sheet or later aeolian dune deposition; it may thus record aggradational geometries. Moreover, this current study only considers aeolian deposits interpreted to have accumulated in response to unimodal wind regime, as has been widely demonstrated for aeolian successions of Cutler Group (Loope, 1981, 1984; Langford & Chan, 1993; Mountney & Jagger, 2004; Taggart et al., 2010). However, elsewhere, ancient aeolian systems associated to bimodal wind regimes are also reported (e.g., Scherer & Goldberg, 2010). In such systems, although the general paleoenvironmental

significance of architectural elements should be similar, their geometries observed in cross-section might diverge from some of the schematic panels presented in this study. Future investigations of the preserved relics of a variety of aeolian-fluvial interaction types should explore how aeolian topography may influence architectural-element geometries through different ranges of alternative sediment accumulation models and wind regime characteristics.

This generalized classification scheme can be applied to help better characterize subsurface sedimentary successions of aeolian-fluvial origin. For example, results presented here can be applied to help make better informed predictions of the composition, geometry and distribution of low-permeability facies and architectural elements present in mixed aeolian-fluvial subsurface successions. Such low-permeability units form significant barriers or baffles to fluid flow and dictate flow pathways in subsurface reservoirs (Meadows & Beach, 1993). Of particular note, characterizing these elements is especially important to predict the performance of subsurface reservoir successions currently being considered as sites for long-term carbon sequestration (e.g., Shipton et al., 2005; Behzadi et al., 2012; Hollingworth et al., 2018; Wheatley et al., 2020).

## 6. Conclusions

Many arid environments are subject to complex geomorphic interactions between aeolian and fluvial processes that lead to a variety of mechanisms of sediment accumulation. Past studies of the stratigraphic units of the Permian Cutler Group in the Paradox Basin have revealed numerous sedimentary architectural relationships to demonstrate the action of competing aeolian-fluvial sedimentation at the time of deposition. A generalized classification scheme for sedimentary architectures arising from such interactions has been devised as an outcome of this study based on the analysis of stratal relationships recorded in 521 outcropping examples of architectural elements recorded and depicted in 24 measured stratigraphic panels. Quantitative trends for element dimensions and geometries are proposed, as are schematic cross-sections depicting key stratal relationships. Eight interaction types are identified: (i) water-table-controlled interdune sedimentation; (ii) deposits originating from low-energy fluvial flood input; (iii) isolated ribbon-shaped fluvial channel-fills originating from episodic confined flooding of interdunes in orientations parallel to the trend of dune crestlines; (iv) isolated ribbon-shaped fluvial channel-fills originating from episodic confined flooding of interdune corridors in orientations perpendicular to the trend of dune crestlines; (v) amalgamated channel elements resulting from persistent, long-lived but confined flooding; (vi) deposits of unconfined sheet-like flood; (vii) fluvial breaching of dunes and their reworking by catastrophic flooding; (viii) aeolian reworking of fluvial deposits.

The preserved sedimentary record of these 8 types of aeolian-fluvial interaction are common not only in in the Cutler Group succession examined as part of this study, but also in mixed aeolian-fluvial sedimentary successions more generally. Criteria set out in this study for the recognition of the 8 types of interaction defined in this novel classification scheme, and the quantitative data summarizing the geometry and facies composition of each type of interaction, can be applied in numerous ways. In particular, the scheme can be applied for (i) determination and reconstruction of the palaeoenvironmental significance of the sedimentary record; (ii) improved characterization and stratigraphic prediction of subsurface successions that might act as hosts for natural resources, including groundwater, oil and gas, and metalliferous ores, else which are of value in geothermal

energy production, or long-term underground sequestration of carbon to mitigate the effect of climate change.

**Acknowledgements**

*Author A* is grateful to the late Bernard Pittet, Professor of Sedimentology at Université Claude Bernard Lyon 1, France, for research discussions. *Author B* thanks Alison Jagger, Oliver Jordan, Stephen Cain, Oliver Wakefield and FRG-ERG-SMRG colleagues for discussions of the palaeoenvironmental significance of the sedimentary record of the Permian Cutler Group. *Author B* also gratefully acknowledges AkerBP, Areva (now Orano), BHP, Cairn India (Vedanta), Chevron, CNOOC International, ConocoPhillips, Equinor, Murphy Oil, Occidental, Petrotechnical Data Systems, Saudi Aramco, Shell, Tullow Oil, Woodside and YPF for their support of the Fluvial, Eolian & Shallow-Marine Research Group at the University of Leeds. This research did not receive any specific grant from funding agencies in the public, commercial, or not-for-profit sectors.

**References**

Ahmed Benan, C.A., Kocurek, G., 2000. Catastrophic flooding of an aeolian dune field: Jurassic Entrada and Todilto formations, Ghost Ranch, New Mexico, USA. Sedimentology 47, 1069–1080. https://doi.org/10.1046/j.1365-3091.2000.00341.x

Al Farraj, A., Harvey, A.M., 2004. Late Quaternary interactions between aeolian and fluvial processes: a case study in the northern UAE. Journal of Arid Environments 56, 235–248. https://doi.org/10.1016/S0140-1963(03)00054-5

Al-Masrahy, M.A., Mountney, N.P., 2015. A classification scheme for fluvial–aeolian system interaction in desert-margin settings. Aeolian Research 17, 67–88. https://doi.org/10.1016/j.aeolia.2015.01.010

Behzadi, H., Alvarado, V., Lynds, R., 2012. Modeling CO2 saturation distribution in eolian systems. International Journal of Greenhouse Gas Control 11, 110–116. https://doi.org/10.1016/j.ijggc.2012.08.004

Bernárdez, S.S., Medina, P.Z., Limarino, C., Bonomo, N., Osella, A., 2021. Fluvial-aeolian interaction deposits in the Andean Foreland basin (Northwest Argentina): Architecture and facies model. Aeolian Research 100754. https://doi.org/10.1016/j.aeolia.2021.100754

Bloomfield, J.P., Moreau, M.F., Newell, A.J., 2006. Characterization of permeability distributions in six lithofacies from the Helsby and Wilmslow sandstone formations of the Cheshire Basin, UK. Geological Society, London, Special Publications 263, 83–101. https://doi.org/10.1144/GSL.SP.2006.263.01.04

Bongiolo, D.E., Scherer, C.M., 2010. Facies architecture and heterogeneity of the fluvial–aeolian reservoirs of the Sergi Formation (Upper Jurassic), Recôncavo Basin, NE Brazil. Marine and Petroleum Geology 27, 1885–1897. https://doi.org/10.1016/j.marpetgeo.2010.07.015

Bullard, J.E., Livingstone, I., 2002. Interactions between aeolian and fluvial systems in dryland environments. Area 34, 8–16. https://doi.org/10.1111/1475-4762.00052

Bullard, J.E., McTainsh, G.H., 2003. Aeolian-fluvial interactions in dryland environments: examples, concepts and Australia case study. Progress in Physical Geography 27, 471–501. https://doi.org/10.1191%2F0309133303pp386ra

Cain, S., 2009. Sedimentology and stratigraphy of a terminal fluvial fan system: the Permian Organ Rock Formation, South East Utah (PhD Thesis). Keele University. https://ethos.bl.uk/OrderDetails.do?uin=uk.bl.ethos.518336

Cain, S.A., Mountney, N.P., 2011. Downstream Changes and Associated Fluvial-Eolian Interactions in an Ancient Terminal Fluvial SystemThe Permian Organ Rock Formation, Se Utah, U.S.A., in: From River to Rock Record, The Preservation of Fluvial Sediments and Their Subsequent Interpretation. SEPM Society for Sedimentary Geology. https://doi.org/10.2110/sepmsp.097.167

Cain, S.A., Mountney, N.P., 2009. Spatial and temporal evolution of a terminal fluvial fan system: the Permian Organ Rock Formation, South-east Utah, USA. Sedimentology 56, 1774–1800. https://doi.org/10.1111/j.1365-3091.2009.01057.x

Carr-Crabaugh, M., Kocurek, G., 1998. Continental sequence stratigraphy of a wet eolian system: a key to relative sea-level change.

Chakraborty, T., Chaudhuri, A.K., 1993. Fluvial-aeolian interactions in a proterozoic alluvial plain: example from the Mancheral quartzite, Sullavai group, Pranhita-Godavari valley, India. Geological Society, London, Special Publications 72, 127–141. https://doi.org/10.1144/GSL.SP.1993.072.01.12

Chan, M.A., 1989. Erg margin of the Permian white rim sandstone, SE Utah. Sedimentology 36, 235–251. https://doi.org/10.1111/j.1365-3091.1989.tb00605.x

Clemmensen, L.B., Abrahamsen, K., 1983. Aeolian stratification and facies association in desert sediments, Arran basin (Permian), Scotland. Sedimentology 30, 311–339. https://doi.org/10.1111/j.1365-3091.1983.tb00676.x

Clemmensen, L.B., Olsen, H., Blakey, R.C., 1989. Erg-margin deposits in the Lower Jurassic Moenave Formation and Wingate Sandstone, southern Utah. Geological Society of America Bulletin 101, 759–773. https://doi.org/10.1130/0016-7606(1989)101%3C0759:EMDITL%3E2.3.CO;2

Condon, S.M., 1997. Geology of the Pennsylvanian and Permian cutler group and Permian Kaibab limestone in the Paradox Basin, southeastern Utah and southwestern Colorado. US Government Printing Office.

Cowan, G., 1993. Identification and significance of aeolian deposits within the dominantly fluvial Sherwood Sandstone Group of the East Irish Sea Basin UK. Geological Society, London, Special Publications 73, 231–245. https://doi.org/10.1144/GSL.SP.1993.073.01.14

Crabaugh, M., Kocurek, G., 1993. Entrada Sandstone: an example of a wet aeolian system. Geological Society, London, Special Publications 72, 103–126. https://doi.org/10.1144/GSL.SP.1993.072.01.11

Demko, T.M., Currie, B.S., Nicoll, K.A., 2004. Regional paleoclimatic and stratigraphic implications of paleosols and fluvial/overbank architecture in the Morrison Formation (Upper Jurassic), Western Interior, USA. Sedimentary Geology 167, 115–135. https://doi.org/10.1016/j.sedgeo.2004.01.003

Driese, S.G., 1985. Interdune pond carbonates, Weber Sandstone (Pennsylvanian-Permian), northern Utah and Colorado. Journal of Sedimentary Research 55, 187–195. https://doi.org/10.1306/212F8661-2B24-11D7-8648000102C1865D

Ellis, D., 1993. The Rough Gas Field: distribution of Permian aeolian and non-aeolian reservoir facies and their impact on field development. Geological Society, London, Special Publications 73, 265–277. https://doi.org/10.1144/GSL.SP.1993.073.01.16

Feder, A., Zimmermann, R., Stollhofen, H., Caracciolo, L., Garzanti, E., Andreani, L., 2018. Fluvial-aeolian sedimentary facies, Sossusvlei, Namib Desert. Journal of Maps 14, 630–643. https://doi.org/10.1080/17445647.2018.1526719

Ferronatto, J.P.F., dos Santos Scherer, C.M., de Souza, E.G., dos Reis, A.D., de Mello, R.G., 2019. Genetic units and facies architecture of a Lower Cretaceous fluvial-aeolian succession, São Sebastião Formation, Jatobá Basin, Brazil. Journal of South American Earth Sciences 89, 158–172. https://doi.org/10.1016/j.jsames.2018.11.009

Frederiksen, K.S., Clemmensen, L.B., Lawaetz, H.S., 1998. Sequential architecture and cyclicity in Permian desert deposits, Brodick Beds, Arran, Scotland. Journal of the Geological Society 155, 677–683. https://doi.org/10.1144/gsjgs.155.4.0677

Geehan, G. & Underwood, J. 1993. The use of length distributions in geological modelling. In: Flint, S.S. & Bryant, I.D. (eds.) The Geological Modelling of Hydrocarbon Reservoirs and Outcrop Analogues. IAS Special Publication, 15, 205-212. https://doi.org/10.1002/9781444303957.ch13

Gradziński, R., Jerzykiewicz, T., 1974. Dinosaur-and mammal-bearing aeolian and associated deposits of the Upper Cretaceous in the Gobi Desert (Mongolia). Sedimentary Geology 12, 249–278. https://doi.org/10.1016/0037-0738(74)90021-9

Haig, D.B., Pickering, S.C., Probert, R., 1997. The Lennox oil and gas field. Geological Society, London, Special Publications 124, 417–436. https://doi.org/10.1144/GSL.SP.1997.124.01.25

Herries, R.D., 1993. Contrasting styles of fluvial-aeolian interaction at a downwind erg margin: Jurassic Kayenta-Navajo transition, northeastern Arizona, USA. Geological Society, London, Special Publications 73, 199–218. https://doi.org/10.1144/GSL.SP.1993.073.01.12

Herries, R.D., Cowan, G., 1997. Challenging the 'sheetflood'myth: the role of water-table-controlled sabkha deposits in redefining the depositional model for the Ormskirk Sandstone Formation (Lower Triassic), East Irish Sea Basin. Geological Society, London, Special Publications 124, 253–276. https://doi.org/10.1144/GSL.SP.1997.124.01.16

Hollands, C.B., Nanson, G.C., Jones, B.G., Bristow, C.S., Price, D.M., Pietsch, T.J., 2006. Aeolian–fluvial interaction: evidence for Late Quaternary channel change and wind-rift linear dune formation in the northwestern Simpson Desert, Australia. Quaternary Science Reviews 25, 142–162. https://doi.org/10.1016/j.quascirev.2005.02.007

Hollingworth, S., Wheatley, D.F., Chan, M.A., Steele, P.A., 2018. Reservoir Characterization of the Permian White Rim Sandstone: Outcrop and Core Assessment for Carbon Capture and Sequestration, in: AAPG ACE 2018.

Hummel, G., Kocurek, G., 1984. Interdune areas of the back-island dune field, North Padre Island, Texas. Sedimentary Geology 39, 1–26. https://doi.org/10.1016/0037-0738(84)90022-8

Huntoon, J.E., Chan, M.A., 1987. Marine origin of paleotopographic relief on eolian White Rim Sandstone (Permian), Elaterite basin, Utah. AAPG Bulletin 71, 1035–1045. https://doi.org/10.1306/703C7DEF-1707-11D7-8645000102C1865D

Jagger, A., 2003. Sedimentology and Stratigraphic Evolution of the Permian Cedar Mesa Sandstone, Paradox Basin, SE Utah (PhD Thesis). University of Keele. https://ethos.bl.uk/OrderDetails.do?uin=uk.bl.ethos.288427

Jones, L.S., Blakey, R.C., 1997. Eolian-fluvial interaction in the Page Sandstone (Middle Jurassic) in south-central Utah, USA—a case study of erg-margin processes. Sedimentary Geology 109, 181–198. https://doi.org/10.1016/S0037-0738(96)00044-9

Jordan, O.D., Mountney, N.P., 2012. Sequence stratigraphic evolution and cyclicity of an ancient coastal desert system: the Pennsylvanian–Permian Lower Cutler Beds, Paradox Basin, Utah, USA. Journal of Sedimentary Research 82, 755–780. https://doi.org/10.2110/jsr.2012.54

Jordan, O.D., Mountney, N.P., 2010. Styles of interaction between aeolian, fluvial and shallow marine environments in the Pennsylvanian to Permian lower Cutler beds, south-east Utah, USA. Sedimentology 57, 1357–1385. https://doi.org/10.1111/j.1365-3091.2010.01148.x

Kamola, D.L., Chan, M.A., 1988. Coastal dune facies, Permian Cutler Formation (White Rim Sandstone), Capitol Reef National Park area, southern Utah. Sedimentary Geology 56, 341–356. https://doi.org/10.1016/0037-0738(88)90060-7

Kocurek, G., 1981. Significance of interdune deposits and bounding surfaces in aeolian dune sands. Sedimentology 28, 753–780. https://doi.org/10.1111/j.1365-3091.1981.tb01941.x

Kocurek, G., Havholm, K.G., 1993. Eolian Sequence Stratigraphy—A Conceptual Framework, in: Siliciclastic Sequence Stratigraphy: Recent Developments and Applications. AAPG Special Volumes, pp. 393–409.

Kocurek, G. and Lancaster, N., 1999. Aeolian system sediment state: theory and Mojave Desert Kelso dune field example. Sedimentology 46, 505-515. https://doi.org/10.1046/j.1365-3091.1999.00227.x

Kocurek, G., Townsley, M., Yeh, E., Havholm, K.G., Sweet, M.L., 1992. Dune and dune-field development on Padre Island, Texas, with implications for interdune deposition and water-table-controlled accumulation. Journal of Sedimentary Research 62, 622–635. https://doi.org/10.1306/D4267974-2B26-11D7-8648000102C1865D

Krapf, C.B., Stollhofen, H., Stanistreet, I.G., 2003. Contrasting styles of ephemeral river systems and their interaction with dunes of the Skeleton Coast erg (Namibia). Quaternary International 104, 41–52. https://doi.org/10.1016/S1040-6182(02)00134-9

Langford, R.P., Chan, M.A., 1988. Flood surfaces and deflation surfaces within the Cutler Formation and Cedar Mesa Sandstone (Permian), southeastern Utah. Geological Society of America Bulletin 100, 1541–1549. https://doi.org/10.1130/0016-7606(1988)100%3C1541:FSADSW%3E2.3.CO;2

Langford, R.P., 1989. Fluvial-aeolian interactions: Part I, modern systems. Sedimentology 36, 1023–1035. https://doi.org/10.1111/j.1365-3091.1989.tb01540.x

Langford, R.P., Chan, M.A., 1989. Fluvial-aeolian interactions: Part II, ancient systems. Sedimentology 36, 1037–1051. https://doi.org/10.1111/j.1365-3091.1989.tb01541.x

Langford, R.P., Chan, M.A., 1993. Downwind changes within an ancient dune sea, Permian Cedar Mesa Sandstone, southeast Utah. Aeolian Sediments: Ancient and Modern 109–126. https://doi.org/10.1002/9781444303971.ch8

Langford, R.P., Pearson, K.M., Duncan, K.A., Tatum, D.M., Adams, L., Depret, P.-A., 2008. Eolian topography as a control on deposition incorporating lessons from modern dune seas: Permian Cedar Mesa Sandstone, SE Utah, USA. Journal of Sedimentary Research 78, 410–422. https://doi.org/10.2110/jsr.2008.045

Liu, B., Coulthard, T.J., 2015. Mapping the interactions between rivers and sand dunes: implications for fluvial and aeolian geomorphology. Geomorphology 231, 246–257. https://doi.org/10.1016/j.geomorph.2014.12.011

Liu, L., Gurnis, M., 2010. Dynamic subsidence and uplift of the Colorado Plateau. Geology 38, 663–666. https://doi.org/10.1130/G30624.1

Loope, D.B., 1981. Deposition, deflation and diagenesis of Upper Paleozoic eolian sediments, Canyonlands National Park, Utah. Unpublished PhD thesis, Laramie, University of Wyoming, 170 pp.

Loope, D.B., 1984. Eolian origin of upper Paleozoic sandstones, southeastern Utah. Journal of Sedimentary Research 54, 563–580. https://doi.org/10.1306/212F846D-2B24-11D7-8648000102C1865D

Loope, D.B., 1985. Episodic deposition and preservation of eolian sands: A late Paleozoic example from southeastern Utah. Geology 13, 73–76. https://doi.org/10.1130/0091-7613(1985)13%3C73:EDAPOE%3E2.0.CO;2

Loope, D.B., Mason, J.A., Dingus, L., 1999. Lethal sandslides from eolian dunes. The Journal of geology 107, 707–713. https://doi.org/10.1086/314377

Loope, D.B., Sanderson, G.A., Verville, G.J., 1990. Abandonment of the name Elephant Canyon Formation in southeastern Utah: physical and temporal implications. Mountain Geologist 27, 119–130.

Mack, G.H., 1979. Littoral marine depositional model for the Cedar Mesa Sandstone (Permian), Canyonlands National Park, Utah, in: Baars, D. L. (Ed.), Permianland — A Field Symposium, Ninth Field Conference. Four Corners Gelogical Society, pp. 33–37.

Meadows, N.S., Beach, A., 1993. Structural and climatic controls on facies distribution in a mixed fluvial and aeolian reservoir: the Triassic Sherwood Sandstone in the Irish Sea. Geological Society, London, Special Publications 73, 247–264. https://doi.org/10.1144/GSL.SP.1993.073.01.15

Middleton, L.T., Blakey, R.C., 1983. Processes and controls on the intertonguing of the Kayenta and Navajo Formations, northern Arizona: eolian-fluvial interactions, in: Developments in Sedimentology. Elsevier, pp. 613–634. https://doi.org/10.1016/S0070-4571(08)70815-X

Mountney, N., Howell, J., Flint, S., Jerram, D., 1998. Aeolian and alluvial deposition within the Mesozoic Etjo Sandstone Formation, northwest Namibia. Journal of African Earth Sciences 27, 175–192. https://doi.org/10.1016/S0899-5362(98)00056-6

Mountney, N.P., 2012. A stratigraphic model to account for complexity in aeolian dune and interdune successions. Sedimentology 59, 964–989. https://doi.org/10.1111/j.1365-3091.2011.01287.x

Mountney, N.P., 2006a. Eolian facies models, in: Posamentier, H.W., Walker, R.G. (Eds.), Facies Models Revisited. SEPM Memoir, pp. 19–83.

Mountney, N.P., 2006b. Periodic accumulation and destruction of aeolian erg sequences in the Permian Cedar Mesa Sandstone, White Canyon, southern Utah, USA. Sedimentology 53, 789–823. https://doi.org/10.1111/j.1365-3091.2006.00793.x

Mountney, N.P., Jagger, A., 2004. Stratigraphic evolution of an aeolian erg margin system: the Permian Cedar Mesa Sandstone, SE Utah, USA. Sedimentology 51, 713–743. https://doi.org/10.1111/j.1365-3091.2004.00646.x

Mountney, N.P., Russell, A.J., 2009. Aeolian dune-field development in a water table-controlled system: Skeiðjarársandur, Southern Iceland. Sedimentology 56, 2107–2131. https://doi.org/10.1111/j.1365-3091.2009.01072.x

Mountney, N.P., Russell, A.J., 2006. Coastal aeolian dune development, Solheimasandur, southern Iceland. Sedimentary Geology 192, 167–181. https://doi.org/10.1016/j.sedgeo.2006.04.004

Mountney, N.P., Thompson, D.B., 2002. Stratigraphic evolution and preservation of aeolian dune and damp/wet interdune strata: an example from the Triassic Helsby Sandstone Formation, Cheshire Basin, UK. Sedimentology 49, 805–833. https://doi.org/10.1046/j.1365-3091.2002.00472.x

Newell, A.J., 2001. Bounding surfaces in a mixed aeolian–fluvial system (Rotliegend, Wessex Basin, SW UK). Marine and Petroleum Geology 18, 339–347. https://doi.org/10.1016/S0264-8172(00)00066-0

Nuccio, V.F., Condon, S.M., 1996. Burial and thermal history of the Paradox Basin, Utah and Colorado, and petroleum potential of the middle Pennsylvanian Paradox Formation, in: Huffman, A.C., Lund, W.R., Godwin, L.H. (Eds.), Geology and Resources of the Paradox Basin. Utah Geological Association, pp. 57–76.

Owen, G., Moretti, M., Alfaro, P., 2011. Recognising triggers for soft-sediment deformation: current understanding and future directions. Sedimentary Geology 235, 133–140. https://doi.org/10.1016/j.sedgeo.2010.12.010

Pederson, J.L., Mackley, R.D., Eddleman, J.L., 2002. Colorado Plateau uplift and erosion evaluated using GIS. GSA Today, 12, 4–10.

Porter, M.L., 1987. Sedimentology of an ancient erg margin: the Lower Jurassic Aztec Sandstone, southern Nevada and southern California. Sedimentology 34, 661–680. https://doi.org/10.1111/j.1365-3091.1987.tb00793.x

Priddy, C.L., Clarke, S.M., 2020. The sedimentology of an ephemeral fluvial–aeolian succession. Sedimentology 67, 2392–2425. https://doi.org/10.1111/sed.12706

Pulvertaft, T.C.R., 1985. Aeolian dune and wet interdune sedimentation in the Middle Proterozoic Dala Sandstone, Sweden. Sedimentary geology 44, 93–111. https://doi.org/10.1016/0037-0738(85)90034-X

Rankey, E.C., 1997. Relations between relative changes in sea level and climate shifts: Pennsylvanian–Permian mixed carbonate-siliciclastic strata, western United States. Geological Society of America Bulletin 109, 1089–1100. https://doi.org/10.1130/0016-7606(1997)109%3C1089:RBRCIS%3E2.3.CO;2

Reis, A.D. dos, Scherer, C.M. dos S., Amarante, F.B. do, Rossetti, M. de M.M., Kifumbi, C., de Souza, E.G., Ferronatto, J.P.F., Owen, A., 2019. Sedimentology of the proximal portion of a large-scale, Upper Jurassic fluvial-aeolian system in Paraná Basin, southwestern Gondwana. Journal of South American Earth Sciences 95, 102248. https://doi.org/10.1016/j.jsames.2019.102248

Robinson, C.A., El-Baz, F., Kusky, T.M., Mainguet, M., Dumay, F., Al Suleimani, Z., Al Marjeby, A., 2007. Role of fluvial and structural processes in the formation of the Wahiba Sands, Oman: A remote sensing perspective. Journal of arid environments 69, 676–694. https://doi.org/10.1016/j.jaridenv.2006.11.015

Rubin, D.M., Hunter, R.E., 1985. Why deposits of longitudinal dunes are rarely recognized in the geologic record. Sedimentology 32, 147–157. https://doi.org/10.1111/j.1365-3091.1985.tb00498.x

Rubin, D.M., Hunter, R.E., 1987. Bedform alignment in directionally varying flows. Science 237, 276–278. https://doi.org/10.1126/science.237.4812.276

Rubin, D.M., Ikeda, H., 1990. Flume experiments on the alignment of transverse, oblique, and longitudinal dunes in directionally varying flows. Sedimentology 37, 673–684. https://doi.org/10.1111/j.1365-3091.1990.tb00628.x

Santos, M.G., Hartley, A.J., Mountney, N.P., Peakall, J., Owen, A., Merino, E.R., Assine, M.L., 2019. Meandering rivers in modern desert basins: Implications for channel planform controls and prevegetation rivers. Sedimentary Geology 385, 1–14. https://doi.org/10.1016/j.sedgeo.2019.03.011

Scherer, C.M., Goldberg, K., 2010. Cyclic cross-bedding in the eolian dunes of the Sergi Formation (Upper Jurassic), Recôncavo Basin: Inferences about the wind regime. Palaeogeography, Palaeoclimatology, Palaeoecology 296, 103–110. https://doi.org/10.1016/j.palaeo.2010.06.018

Shipton, Z.K., Evans, J.P., Dockrill, B., Heath, J., Williams, A., Kirchner, D., Kolesar, P.T., Thomas, D.C., Benson, S.M., 2005. Natural leaking $CO_2$-charged systems as analogs for failed geologic storage reservoirs, in: Thomas, D.C., Benson, S.M. (Eds.), Carbon dioxide capture for storage in deep geologic formations. Elsevier Ltd., pp. 699–712.

Simpson, E.L., Hilbert-Wolf, H.L., Simpson, W.S., Tindall, S.E., Bernard, J.J., Jenesky, T.A., Wizevich, M.C., 2008. The interaction of aeolian and fluvial processes during deposition of the Upper Cretaceous capping sandstone member, Wahweap Formation, Kaiparowits Basin, Utah, USA. Palaeogeography, Palaeoclimatology, Palaeoecology 270, 19–28. https://doi.org/10.1016/j.palaeo.2008.08.009

Smith, R.A., Jones, N.S., Monaghan, A.A., Arkley, S., 2006. Fluvial and aeolian deposition in the Siluro-devonian Swanshaw Sandstone Formation, SW Scotland. Scottish Journal of Geology 42, 161–177. https://doi.org/10.1144/sjg42020161

Spalletti, L.A., Limarino, C.O., Colombo Piñol, F., 2010. Internal anatomy of an erg sequence from the aeolian-fluvial system of the De La Cuesta Formation (Paganzo Basin, northwestern Argentina). Geologica Acta 8. https://doi.org/10.1344/105.000001581

Stanesco, J.D., Campbell, J.A., 1989. Eolian and noneolian facies of the lower Permian Cedar Mesa Sandstone Member of the Cutler Formation, southeastern Utah. US Government Printing Office.

Stanesco, J.D., Dubiel, R.F., Huntoon, J.E., 2000. Depositional environments and paleotectonics of the Organ Rock Formation of the Permian Cutler Group, southeastern Utah in, Geology of Utah's national parks and monuments. Utah Geological Association Publication 28, 591–605.

Stanistreet, I.G., Stollhofen, H., 2002. Hoanib River flood deposits of Namib Desert interdunes asanalogues for thin permeability barrier mudstone layers inaeolianite reservoirs. Sedimentology 49, 719–736. https://doi.org/10.1046/j.1365-3091.2002.00458.x

Strömbäck, A., Howell, J.A., Veiga, G.D., 2005. The transgression of an erg—sedimentation and reworking/soft-sediment deformation of aeolian facies: the Cretaceous Troncoso Member, Neuquén Basin, Argentina. Geological Society, London, Special Publications 252, 163–183. https://doi.org/10.1144/GSL.SP.2005.252.01.08

Suter, F., Martínez, J.I., Vélez, M.I., 2011. Holocene soft-sediment deformation of the Santa Fe–Sopetrán Basin, northern Colombian Andes: Evidence for pre-Hispanic seismic activity? Sedimentary Geology 235, 188–199. https://doi.org/10.1016/j.sedgeo.2010.09.018

Svendsen, J., Stollhofen, H., Krapf, C.B., Stanistreet, I.G., 2003. Mass and hyperconcentrated flow deposits record dune damming and catastrophic breakthrough of ephemeral rivers, Skeleton Coast Erg, Namibia. Sedimentary Geology 160, 7–31. https://doi.org/10.1016/S0037-0738(02)00334-2

Sweet, M.P., 1999. Interaction between aeolian, fluvial and playa environments in the Permian Upper Rotliegend Group, UK southern North Sea. Sedimentology 46, 171–187. https://doi.org/10.1046/j.1365-3091.1999.00211.x

Taggart, S., Hampson, G.J., Jackson, M.D., 2010. High-resolution stratigraphic architecture and lithological heterogeneity within marginal aeolian reservoir analogues. Sedimentology 57, 1246–1279. https://doi.org/10.1111/j.1365-3091.2010.01145.x

Teller, J.T., Rutter, N., Lancaster, N., 1990. Sedimentology and paleohydrology of late Quaternary lake deposits in the northern Namib Sand Sea, Namibia. Quaternary Science Reviews 9, 343–364. https://doi.org/10.1016/0277-3791(90)90027-8

Tooth, S., 2000. Process, form and change in dryland rivers: a review of recent research. Earth-Science Reviews 51, 67–107. https://doi.org/10.1016/S0012-8252(00)00014-3

Trewin, N.H., 1993. Controls on fluvial deposition in mixed fluvial and aeolian facies within the Tumblagooda Sandstone (Late Silurian) of Western Australia. Sedimentary Geology 85, 387–400. https://doi.org/10.1016/0037-0738(93)90094-L

Veiga, G.D., Spalletti, L.A., Flint, S., 2002. Aeolian/fluvial interactions and high-resolution sequence stratigraphy of a non-marine lowstand wedge: the Avilé Member of the Agrio Formation (Lower Cretaceous), central Neuquén Basin, Argentina. Sedimentology 49, 1001–1019. https://doi.org/10.1046/j.1365-3091.2002.00487.x

Wakefield, O.J.W., Mountney, N.P., 2013. Stratigraphic architecture of back-filled incised-valley systems: Pennsylvanian–Permian lower Cutler beds, Utah, USA. Sedimentary Geology 298, 1–16. https://doi.org/10.1016/j.sedgeo.2013.10.002

Wakefield, O.J.W., 2010. Aeolian, fluvial and shallow marine sedimentary system interactions in the Permian Cutler group, southeast Utah, USA (PhD Thesis). Keele University. https://ethos.bl.uk/OrderDetails.do?uin=uk.bl.ethos.534308

Wheatley, D., Hollingworth, S., Steele, P., Chan, M., 2020. Sedimentology, diagenesis, and reservoir characterization of the Permian White Rim Sandstone, southern Utah: Implications for carbon capture and sequestration potential. Bulletin 104, 1357–1373. https://doi.org/10.1306/11111918215

## Tables

***Table 1.*** *Notable examples of well-exposed ancient sedimentary formations interpreted to record mixed aeolian-fluvial depositional systems.*

| Litho-stratigraphic unit | Age | Location | Dominant depositional environments | References |
|---|---|---|---|---|
| De La Cuesta Fm. | Permian | Argentina | Aeolian, alluvial fan, mudflat | *Spalletti et al., (2010)* |
| Huitrín Fm. | Cretaceous | Argentina | Aeolian, braided fluvial | *Strömbäck et al., (2005)* |
| Agrio Fm. | Cretaceous | Argentina | Wet-aeolian, fluvial | *Veiga et al., (2002)* |
| Tumblagooda Sandstone | Silurian | Australia | Aeolian, fluvial | *Trewin, (1993)* |
| São Sebastião Fm. | Cretaceous | Brasil | Aeolian, fluvial | *Ferronatto et al., (2019)* |
| Pirambóia Fm. | Jurassic | Brasil | Wet-aeolian, fluvial | *Reis et al., (2019)* |
| Sergi Fm. | Jurassic | Brasil | Aeolian, fluvial, lacustrine | *Bongiolo & Scherer, (2010)* |
| Mancheral Quartzite | Neoproterozoic | India | Aeolian, fluvial | *Chakraborty & Chaudhuri, (1993)* |
| Ormskirk Sandstone | Triassic | Irish Sea and UK | Fluvial, aeolian | *Cowan, (1993); Meadows & Beach, (1993); Haig et al., (1997); Herries & Cowan, (1997)* |
| Barun Goyot Fm. | Cretaceous | Mongolia | Aeolian, fluvial, lacustrine | *Gradziński & Jerzykiewicz, (1974)* |
| Djadokhta Fm. | Cretaceous | Mongolia | Aeolian | *Loope et al., (1999)* |
| Twyfelfontein Fm (including "Etjo Sandstone") | Jurassic | Namibia | Aeolian, fluvial | *Mountney et al., (1998)* |
| Upper Rotliegend Group | Permian | North Sea | Aeolian, fluvial, playa | *Ellis, (1993); Sweet, (1999)* |
| Helsby Sandstone | Triassic | UK | Aeolian, fluvial | *Mountney & Thompson, (2002); Bloomfield et al., (2006)* |
| Brodick Beds | Permian | Arran, UK | Aeolian, fluvial, lacustrine | *Clemmensen & Abrahamsen, (1983); Frederiksen et al., (1998)* |

| | | | | |
|---|---|---|---|---|
| Dawlish Sandstone | Triassic | UK | Aeolian, fluvial | *Newell, (2001)* |
| Swanshaw Sandstone | Siluro-Devonian | UK | Fluvial, Aeolian | *Smith et al., (2006)* |
| Wahweap Fm. | Cretaceous | Utah, USA | Fluvial, aeolian | *Simpson et al., (2008)* |
| Aztec Sandstone | Jurassic | Nevada and California, USA | Aeolian, alluvial fan, sabkha | *Porter, (1987)* |
| Cutler Group | Permian | Colorado Plateau, USA | Aeolian, fluvial | *Loope, (1985); Langford & Chan, (1988, 1989); Mountney & Jagger, (2004); Mountney, (2006b); Cain & Mountney, (2009); Jordan & Mountney, (2012)* |
| Glen Canyon Group | Jurassic | Colorado Plateau, USA | Aeolian, fluvial | *Middleton & Blakey, (1983;) Clemmensen et al., (1989;) Herries, (1993); Jones & Blakey, (1997)* |
| San Rafael Group | Jurassic | Colorado Plateau, USA | Aeolian | *Carr-Crabaugh & Kocurek, (1998); Ahmed Benan & Kocurek, (2000); Priddy & Clarke, (2020)* |

***Table 2.*** *Summary of common lithofacies observed in the studied successions.*

| Facies code | Description | Typical Environmental Setting |
|---|---|---|
| Clc | Thin and nodular carbonate mudstone or wackestone. In some cases with bioclasts of terrestrial invertebrates. In some cases with calcrete nodules. | Evaporitic freshwater limestone |
| Pls | Thin units of clay to silt mudstone with strong colour gradient, rhizoliths, evaporitic minerals and bleaching. | Palaeosol |
| Adu | Fine- to medium-grain sandstone with decimetre- to metre-scale cross bedding. | Aeolian dune |
| Awit | Clay to very fine-grain red sandstone with planar lamination, chert (silcrete), bioturbation, trace-fossils (burrows), evaporitic minerals and soft-sediment deformation structures. | Wet interdune |
| Adit | Silt to very fine-grain red sandstone with wavy lamination, adhesion warts and ripples, calcrete nodules, rhizoliths, burrows and raindrop impact marks. | Damp interdune |
| Assh | Well-sorted very fine- to fine-grain wind-ripple strata and plane-bed strata with planar laminations. | Aeolian sand-sheet |
| Flp | Silt to very fine-grain sandstone with rhizoliths, burrows, calcrete nodules, current and oscillatory ripples. | Overbank floodplain |
| Fedr | Cross-bedded fine-grain sandstone with pebble lags, rhizoliths, burrows, and lamination and structures indicative of lower flow-regime conditions.. | Ephemeral dryland river channel |
| Fldr | Cross-bedded and plane-bedded fine- to medium-grain sandstone with climbing-ripple strata, calcrete nodules, rhizoliths, burrows, bleaching and mottling. | Ephemeral dryland river channel |
| Fsh | Fine- to medium-grain sandstone with upper flow-regime laminations and rhizoliths. | High-energy non-channelised, sheet-like flood |
| Fhc | Massive fine to coarse (rarely very coarse) sandstone with decimetre-scale intraformational sandstone clasts. Rare aqueous ripple strata. | Hyper-concentrated flows. May record Fluvial reworking of aeolian deposits |

| | | |
|---|---|---|
| Fmf | Normally graded very fine- to medium-grain sandstone with soft mudstone-pebbles as floating clasts and soft-sediment deformation structures. | Intra-erg mass flows; fluvial reworking of aeolian deposits |
| Afl | Centimetre-thick layers of fine- to medium-grain sandstone with rare ripple strata. | Aeolian reworking of fluvial deposits |

***Table 3.*** *Summary of architectural elements representing fluvial-aeolian interactions in the studied successions, and their constituent lithofacies.*

| Element code | Architectural element | Facies association | Dominant lithofacies types | Key defining features for identification and/or differentiation |
|---|---|---|---|---|
| WID | Water-table-controlled *wet* interdune element | FA1 | Awit; Pls; Clc | Claystone and siltstone (mudstone); less common fine sandstone; planar lamination; evaporate minerals (especially chert); bioturbation; soft-sediment deformation structures; desiccation cracks; overlapping geometries and interfingering with *Adu* units |
| DID | Water-table-controlled *damp* interdune element | FA2 | Adit; Pls; Clc | Siltstone to fine sandstone; wavy laminations; adhesion structures; rain drop impacts; desiccation cracks; soft-sediment deformation structures; overlapping geometries and interfingering with *Adu* units |
| LED | Low-energy deposit originating from fluvial flood input | FA3 | Flp; Pls; Clc | Siltstone to very fine (rarely medium) sandstone; minor channel scours; asymmetrical current ripple forms on bedding surfaces and current-ripple lamination indicative of unidirectional currents; bidirectional (oscillatory) current ripple forms and stratification; small plant root traces (rhizoliths); bioturbation, trace fossils (burrows); calcrete palaeosols; freshwater limestone beds |
| ICF | Isolated ribbon-shaped channel-fill originating from episodic confined flooding of the interdune | FA4 | Fedr; Flp; Pls; Clc; Assh | Isolated channel-forms enclosed by aeolian units; cross-bedded sets of fluvial origin; asymmetrical current ripple forms on bedding surfaces and current-ripple lamination indicative of unidirectional currents |
| ACF | Amalgamated channel-forms resulting from long-lasting confined flooding of the interdune | FA5 | Fldr; Flp; Pls; Clc | Isolated channel-forms; single story or multi-storey units; multi-lateral units; channel fills composed of locally reworked sediment; intraformational and extraformational pebble clasts |

| | | | | |
|---|---|---|---|---|
| SFD | Unconfined sheet-like flood deposits | FA6 | Fsh; Flp; Pls | Extensive fluvial sandstone overlapping isolated *Adu* units; abundant primary current lineation |
| DR | Dune reworking by fluvial breaching and catastrophic flooding | FA7 | Fhc; Fmf | High-relief incision of *Adu* units; trench-like channel scours; fill of homogenized sand; fill of intraformational rip-up clasts of *Adu* |
| FLR | Aeolian reworking of fluvial deposits | FA8 | Afl | Fine, well-sorted aeolian sandstone laminations and thin beds mantling relic fluvial barform surfaces |

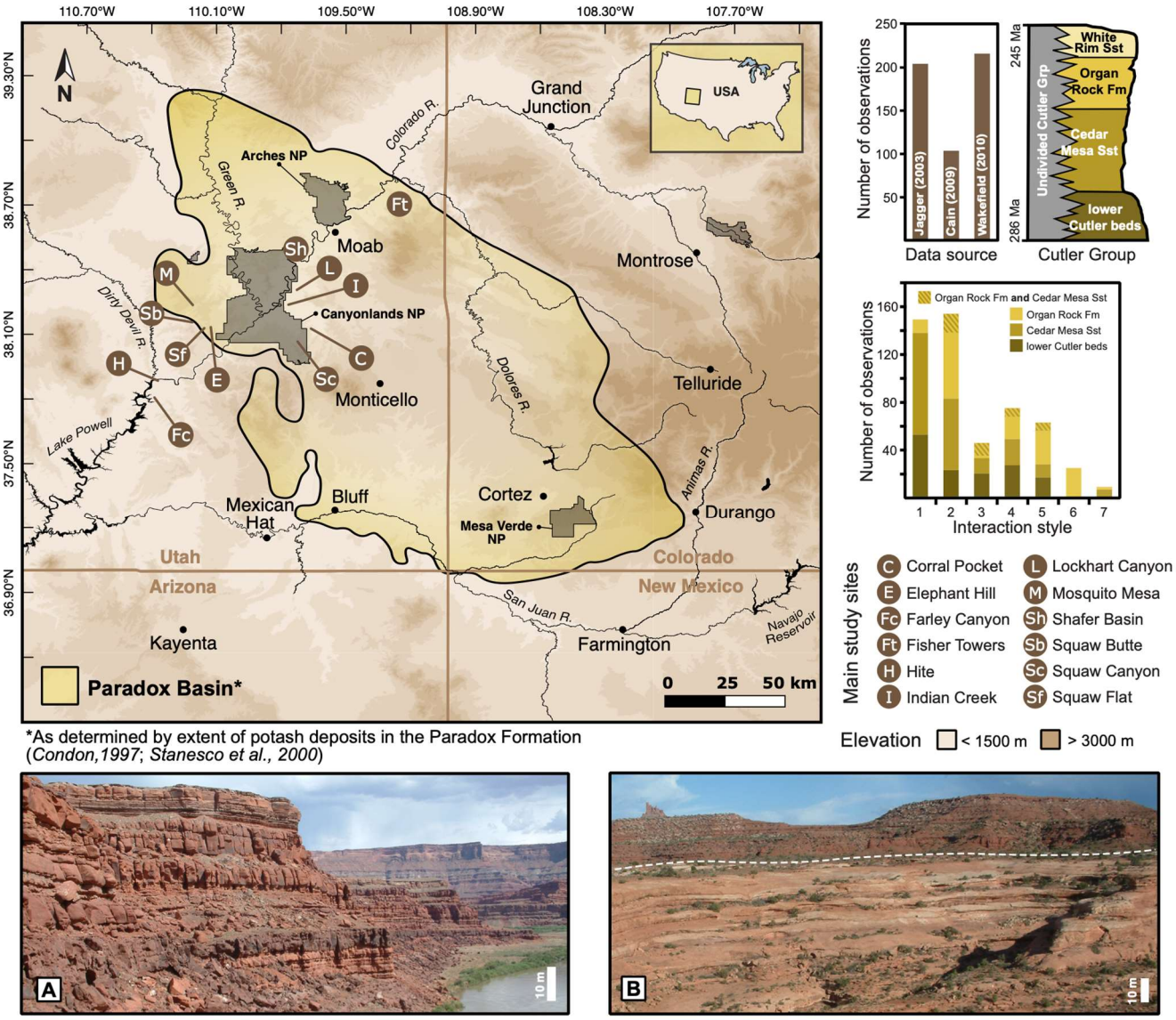


*As determined by extent of potash deposits in the Paradox Formation (*Condon,1997*; *Stanesco et al., 2000*)

## Figures

***FIGURE 1 (2-column fitting).*** *Locations of the main study sites and extent of the Paradox Basin as defined by the distribution of salt deposits of the Paradox Formation that accumulated as an evaporitic marine system in the basin during the Pennsylvanian (Condon, 1997; Stanesco et al., 2000). Map is augmented with data from Wakefield (2010). Elevation data are extracted from the USGS TNM website (https://apps.nationalmap.gov/downloader). Amounts of recorded observations per data source, interaction style and stratigraphic unit are given. Because of the observation scale of FLR elements – centimetre to decimetre, no data has been recorded for interaction style 8. Photograph of the typical outcropping sedimentary architecture of the lower Cutler beds (A) and the Cedar Mesa Sandstone – light orange – overlain by the Organ Rock Formation – dark orange (B).*

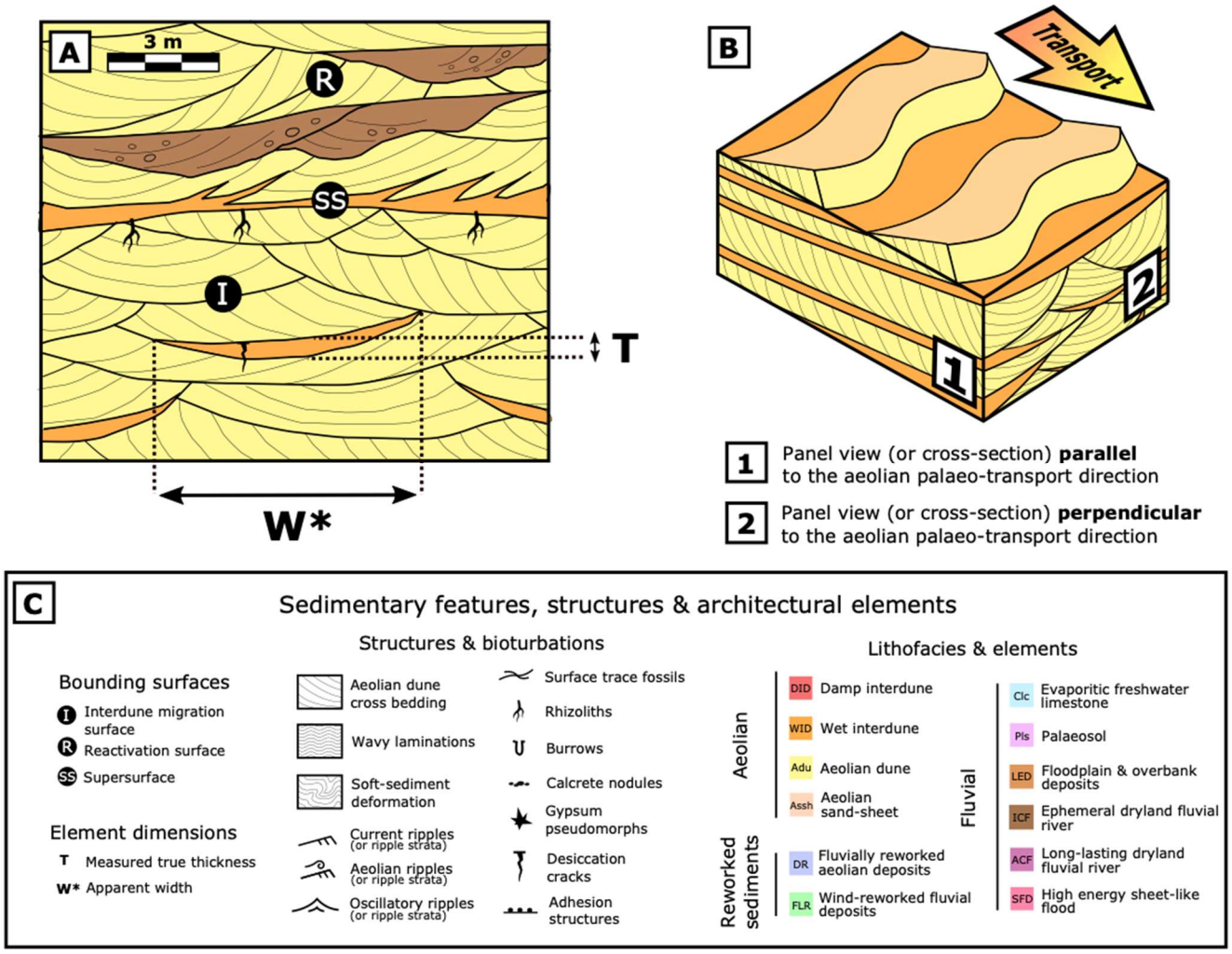


***Figure 2 (2-column fitting).*** *A) Example of part of an architectural panel highlighting the different surface boundaries recorded for aeolian-fluvial successions of the Paradox Basin. The architectural panel is depicted normal to the ground; thus, measured thicknesses of architectural elements are true thicknesses for the point of observation. Measured widths are only apparent and depend on the panel orientation relative to the aeolian palaeo-transport direction, and therefore to the orientation of the original aeolian dune bedforms. B) Schematic diagram of a water-table-controlled aeolian system that has accumulated via bedform climbing, with transport-parallel and transport-perpendicular panel views revealing the form of the preserved deposits. C) Simplified inventory of the different sedimentary features, structures, lithofacies and architectural elements examined as part of the present study.*


2 m
A


B


C


D


20 m
E


F


G


H

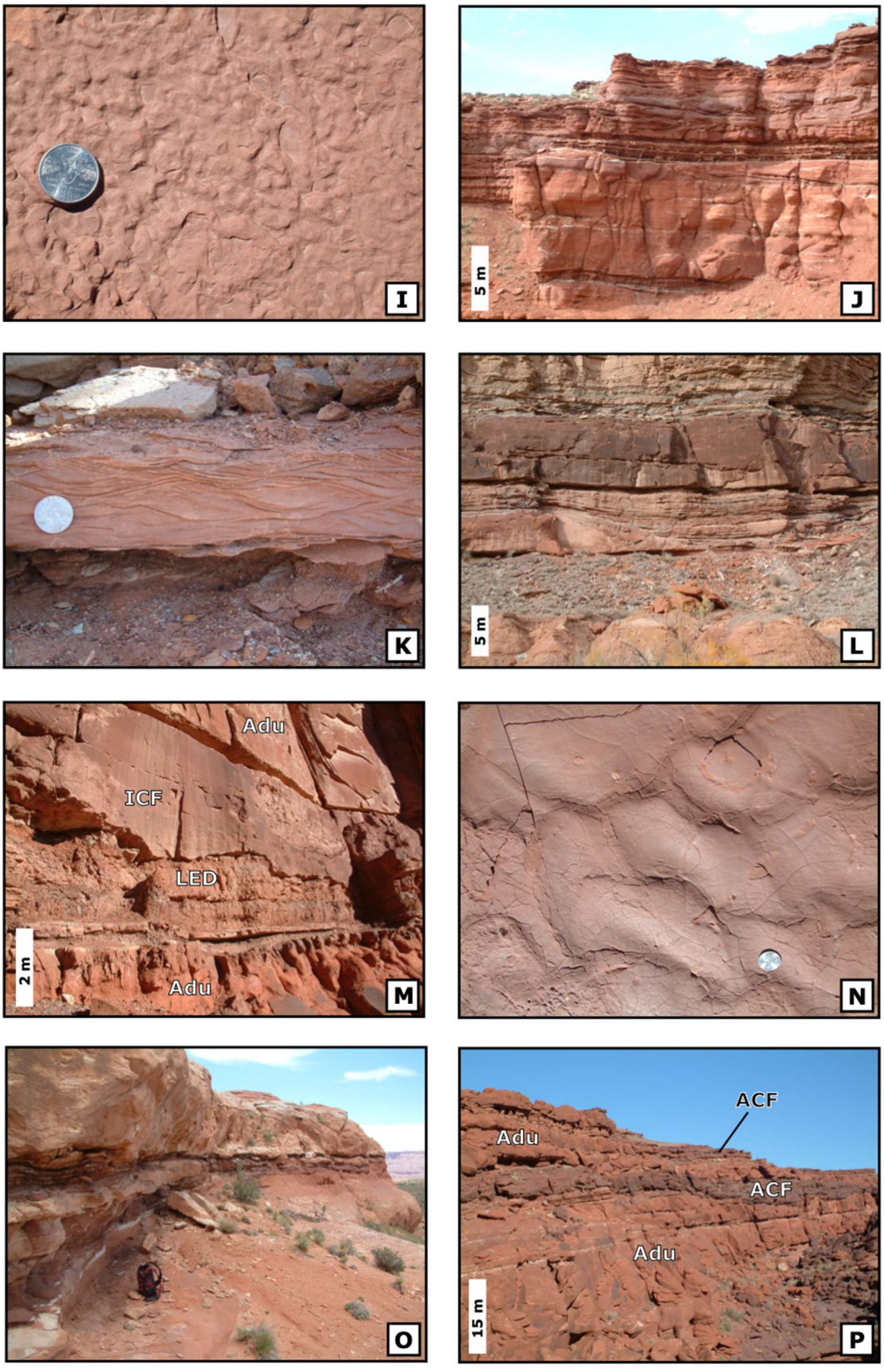
I
5 m
J
K
5 m
L
Adu
ICF
LED
2 m
Adu
M
N
O
ACF
Adu
ACF
Adu
15 m
P


5 m
Q


R


S

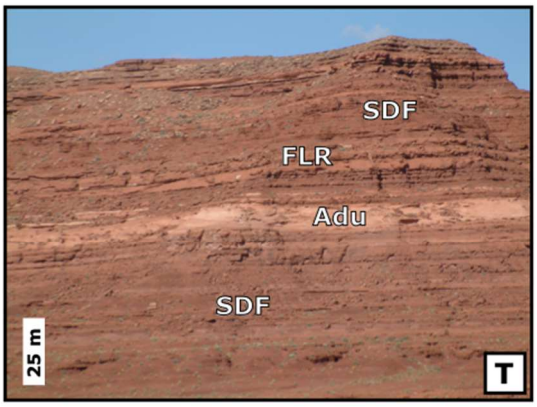
SDF
FLR
Adu
SDF
25 m
T


U

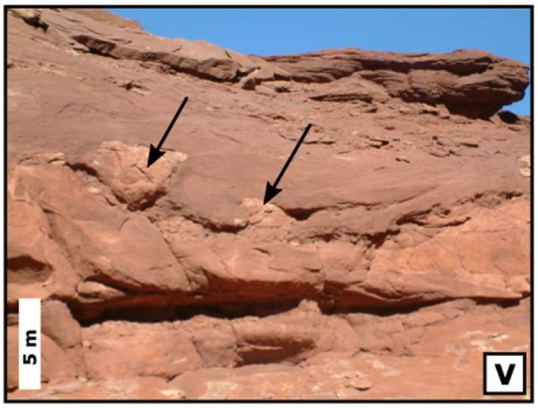
5 m
V

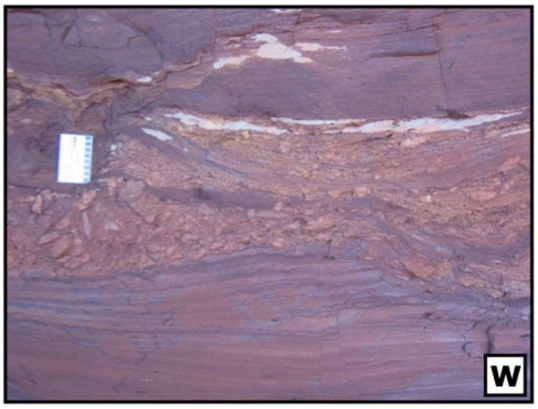
W


X

***FIGURE 3 (2-column fitting).*** *A) transport-perpendicular section of an aeolian dune facies unit (Adu) exhibiting sets of trough cross-bedding as a compound coset, Cedar Mesa Sandstone; B) prominent red mudstone wet interdune pond deposit (WID element) enclosed between Adu units, Cedar Mesa Sandstone; red mudstone bed is 0.25 m thick; C) intertonguing relationship between silty-sandstone deposits of a wet interdune (WID) element and overlying toesets of an aeolian dune (Adu) unit, Cedar Mesa Sandstone; penknife for scale; D) layered chert deposit forming the uppermost part of the fill of a wet interdune (WID) element, Cedar Mesa Sandstone; E) damp interdune (DID) element (arrow indicates position)in a 20 m-thick aeolian sequence, Cedar Mesa Sandstone; F) calcrete palaeosol developed in silty sandstone of a damp interdune (DID) element, Cedar Mesa Sandstone; glove for scale; G) in-situ tree trunk rhizolith preserved in a damp interdune (DID) element, Cedar Mesa Sandstone; penknife for scale; H) bioturbation on a sandstone bedding surface in a damp interdune (DID) element, Cedar Mesa Sandstone; I) adhesion structures preserved on a silty-sandstone bedding surface in a damp interdune (DID) element, Cedar Mesa Sandstone; J) siltstone and fine sandstone (LED element) with current ripples and desiccation cracks between Adu units, Cedar Mesa Sandstone; observed cliff section is 20 m high; K) wave-ripple stratification preserved in a sandstone bed of a LED element, Organ Rock Formation; L) heterolithic strata of an isolated fluvial channel-fill (ICF element) onlapping onto the flanks of a preserved aeolian dune lee; section is oriented perpendicular to aeolian palaeo-transport, which was to the right as viewed; the overlying massive sandstone beds are of an amalgamated channelized (ACF) element; lower Cutler beds; observed cliff section is 20 m high; M) isolated channel-fill (ICF) element with pebble lag filling base of channel; the channel incises into an underlying LED element; Adu units are present a the base and top of the image; lower Cutler beds; observed cliff section is 8 m high; N) linguoid current ripple forms preserved on a sandstone bedding surface; small desiccation cracks and bioturbation are also evident; isolated channel-fill (ICF) element, Organ Rock Formation; O) ICF element preserved between underlying and overlying Adu units, Cedar Mesa Sandstone; rucksack for scale; P) dark purple-brown multilateral- and multi-storey amalgamated channel (ACF) elements interbedded between orange aeolian dune units (Adu), Undivided Cutler Group; observed cliff section is 50 m high; Q) dark purple-brown amalgamated channel (ACF) element with erosive base, Undivided Cutler Group; observed cliff section is 30 m high; R) fluvial cross-bedded sets, some with extraformational pebbles, others with soft-sediment deformation structures, lower Cutler beds; S) fluvial sheet-like (SFD) element bounded by underlying and overlying Adu units, Cedar Mesa Sandstone; T) vertically stacked fluvial sheet-like (SFD) elements (dark orange); a prominent beige-colour aeolian dune sequence (Adu) is present in the centre of the cliff section; aeolian reworked fluvial deposits (probably of loess origin) are preserved as FLR elements (light orange); Organ Rock Formation; observed cliff section is ~150 m high; U) and V) two examples of trench-like fluvial incisions into underlying Adu units; the bases of the channel fills contain reworked aeolian blocks (indicated by arrows); these are DR elements, Organ Rock Formation; rucksack for scale in U; observed cliff section is 20 m high in V; W) sandstone intraclasts of aeolian origin (Fhc facies) preserved in fluvial deposits of a DR element, Organ Rock Formation; X) aeolian reworking of sediments that were likely originally of fluvial origin (FLR element), lower Cutler beds.*

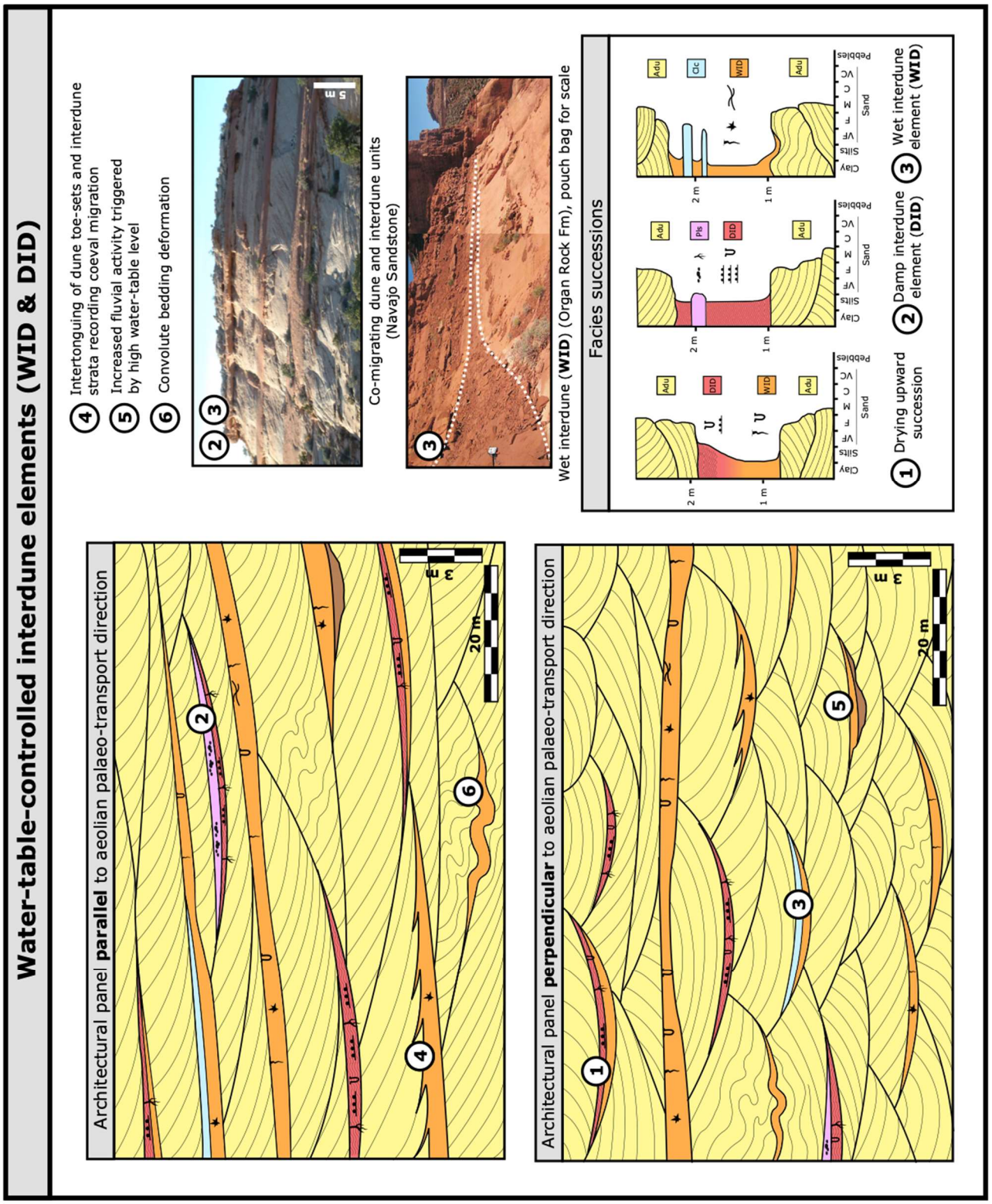


***Figure 4 (2-column fitting).*** *Schematic architectural panels depicting the range of different sedimentary units, elements and geometries symptomatic of preserved water-table-controlled interdune elements (Langford & Chan, 1989; Crabaugh & Kocurek, 1993; Mountney & Jagger, 2004). Key features and idealized successions are shown. In addition to example architectures from the Permian Cutler Group, an example from the Jurassic Navajo Sandstone in southeast Utah is also shown.*

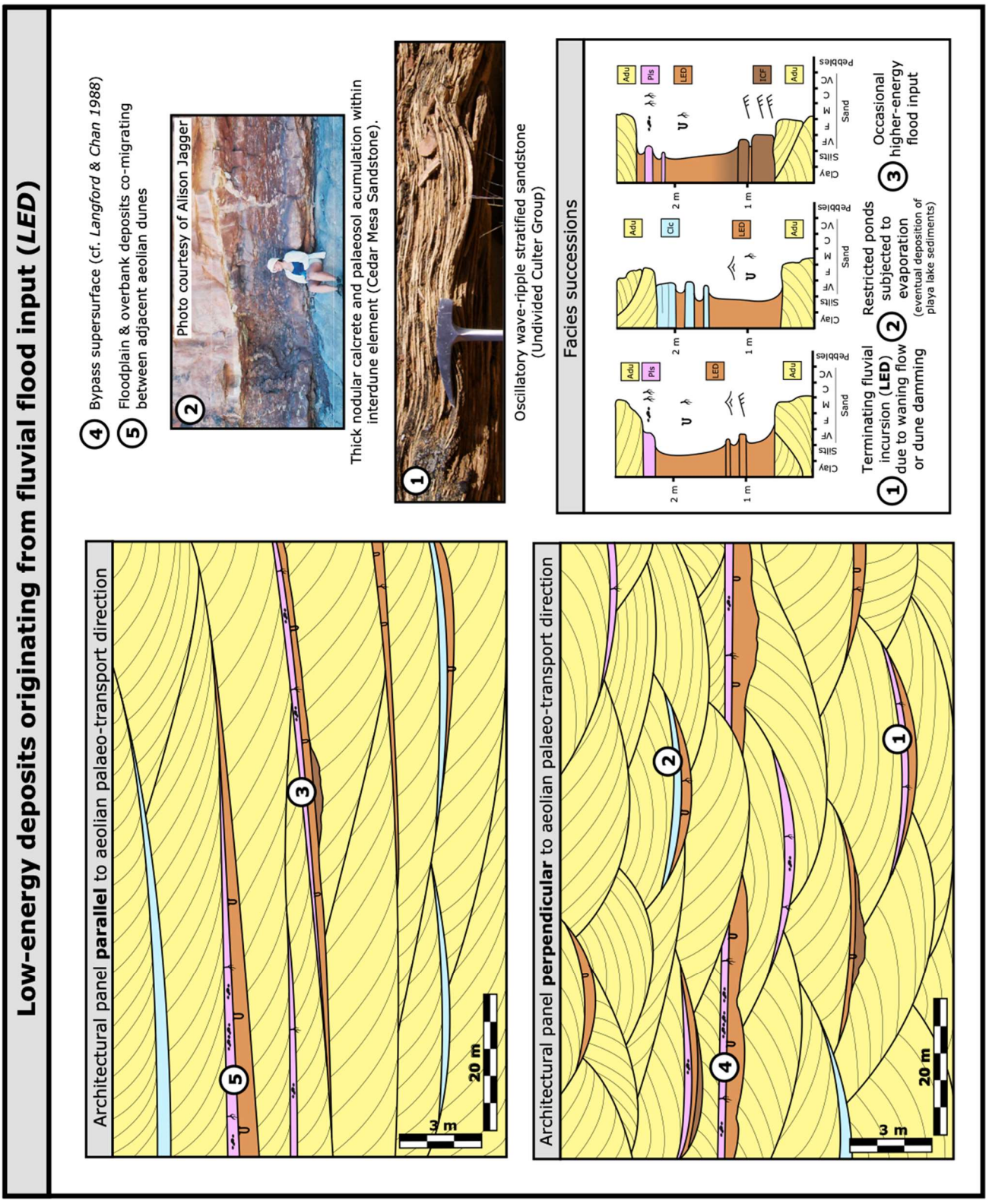


***Figure 5 (2-column fitting).*** *Schematic architectural panels depicting the range of different sedimentary units, elements and geometries symptomatic of interdune restricted low-energy deposition originating from flood input (Langford & Chan, 1989; Mountney, 2006b). Key features and idealized successions are shown.*

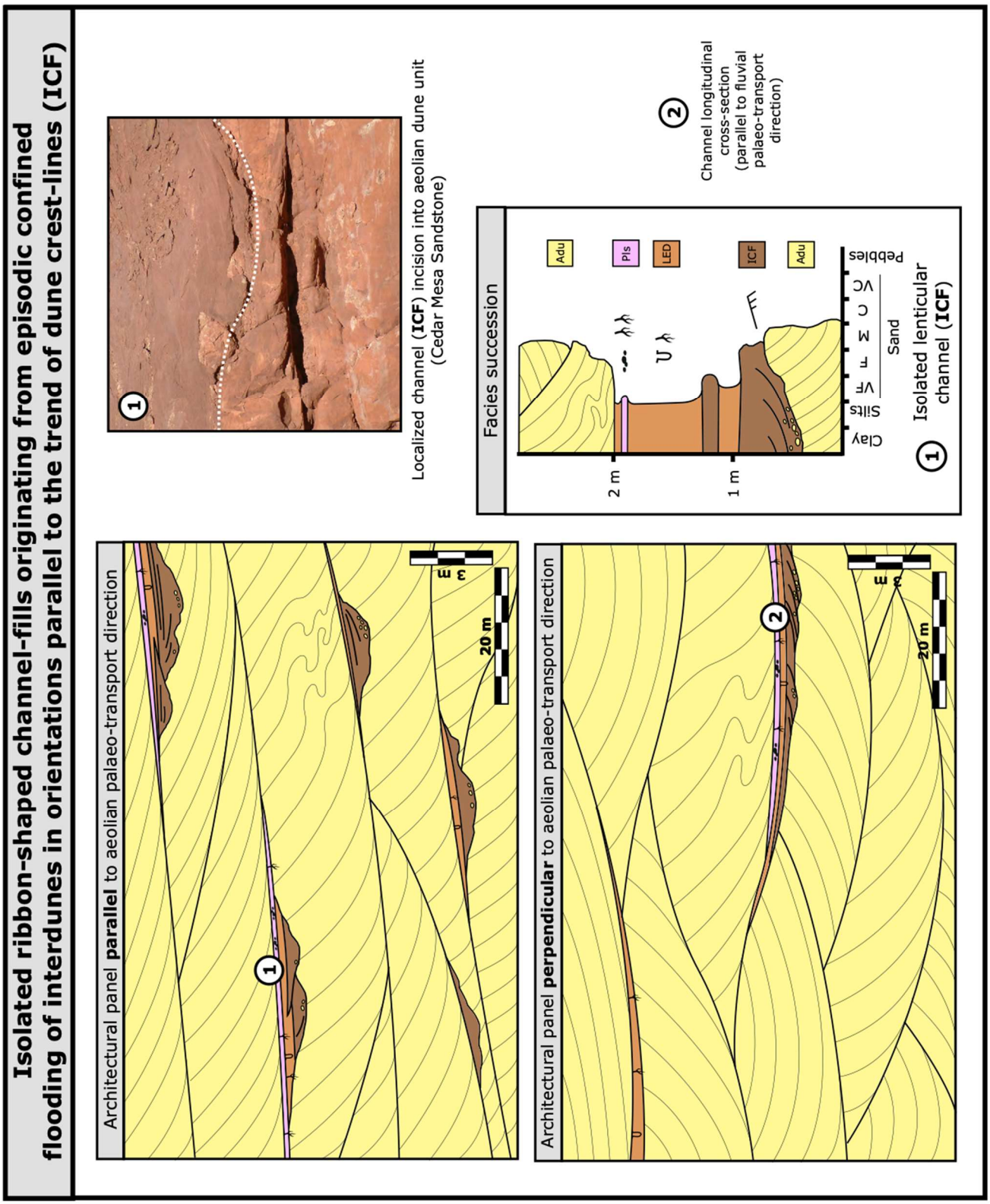


***Figure 6 (2-column fitting).*** *Schematic architectural panels depicting the range of different sedimentary units, elements and geometries symptomatic of episodic fluvial deposition originating from confined flooding in interdune corridors parallel to the dune crest-line trend (Langford & Chan, 1989; Herries, 1993). Key features and idealized successions are shown.*

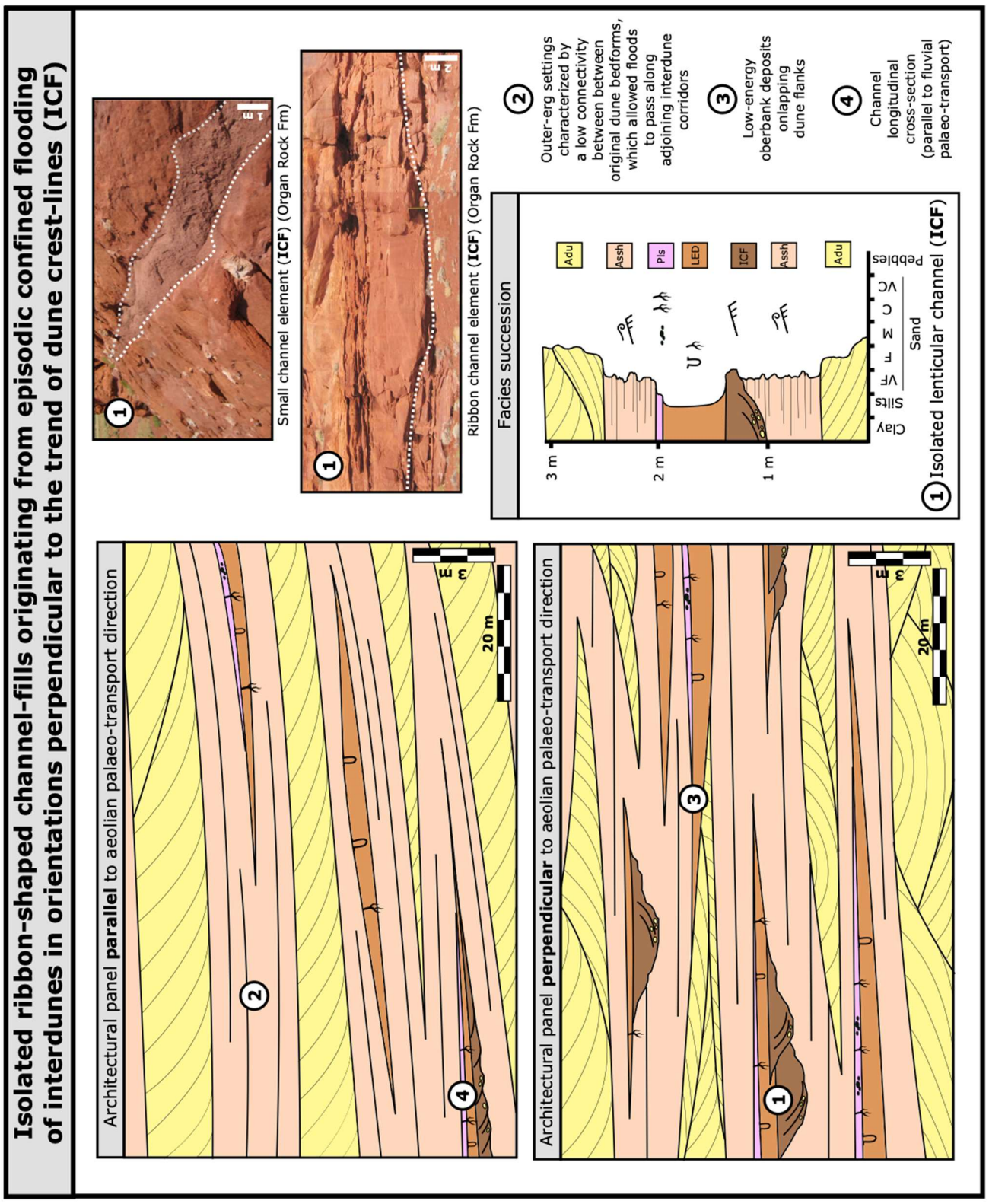


***Figure 7 (2-column fitting).*** *Schematic architectural panels depicting the range of different sedimentary units, elements and geometries symptomatic of episodic fluvial deposition originating from confined flooding in interdune corridors perpendicular to the dune crest-line trend (Langford & Chan, 1989; Herries, 1993). Key features and idealized successions are shown.*

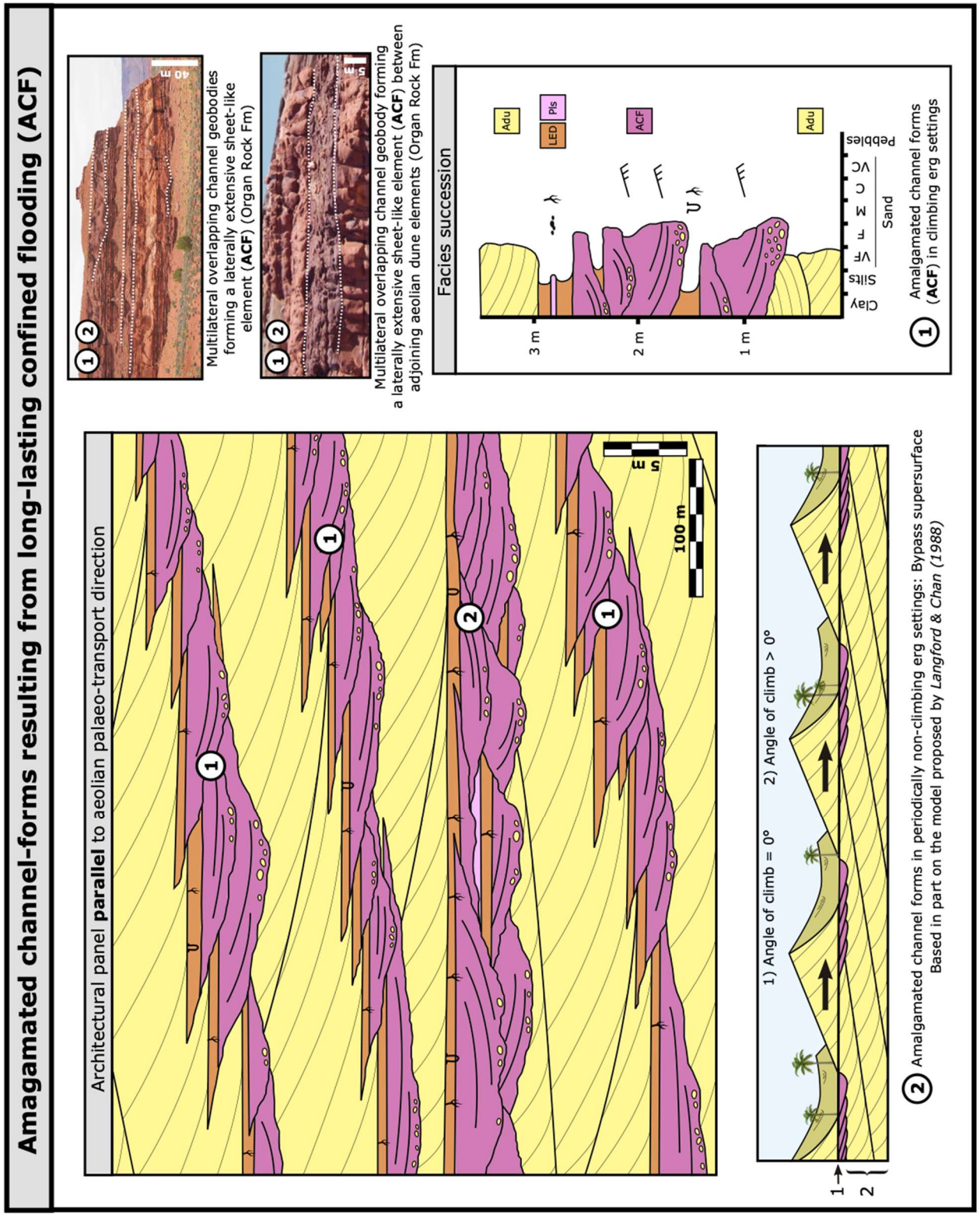


***Figure 8 (2-column fitting).*** *Schematic architectural panel depicting the range of different sedimentary units, elements and geometries symptomatic of long-lived floods confined within interdune corridors (Langford & Chan, 1988, 1989; Herries, 1993; Carr-Crabaugh & Kocurek, 1998; Mountney & Jagger, 2004). Key features and idealized successions are shown. Diagram depicting bypass supersurface generation modified in part from Langford & Chan (1988).*

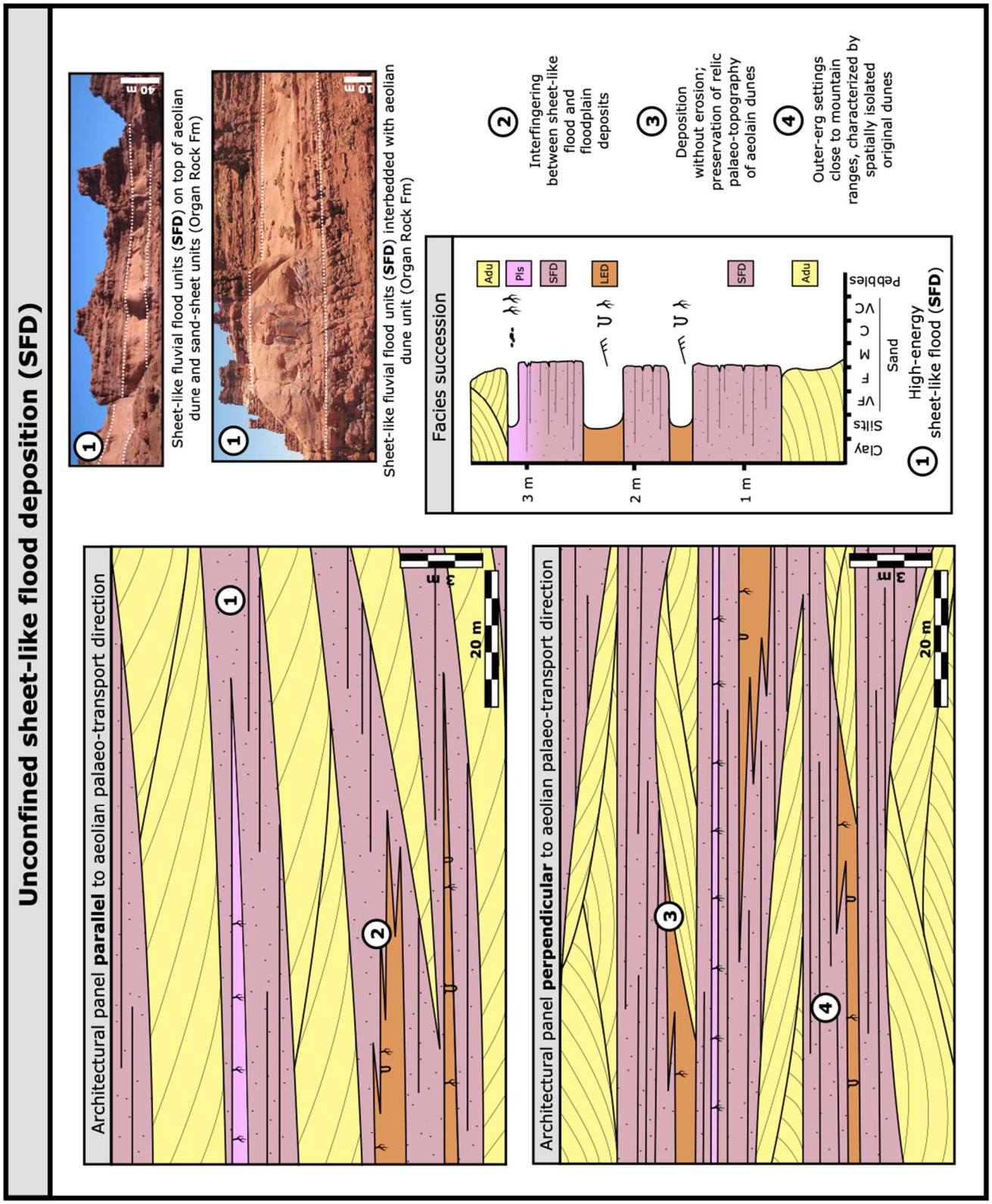


***Figure 9 (2-column fitting).*** *Schematic architectural panels depicting the range of different sedimentary units, elements and geometries symptomatic of unchannelized fluvial deposition in outer-*

*erg settings close to mountain ranges (Mountney & Jagger, 2004; Cain & Mountney, 2011). Key features and idealized successions are shown.*

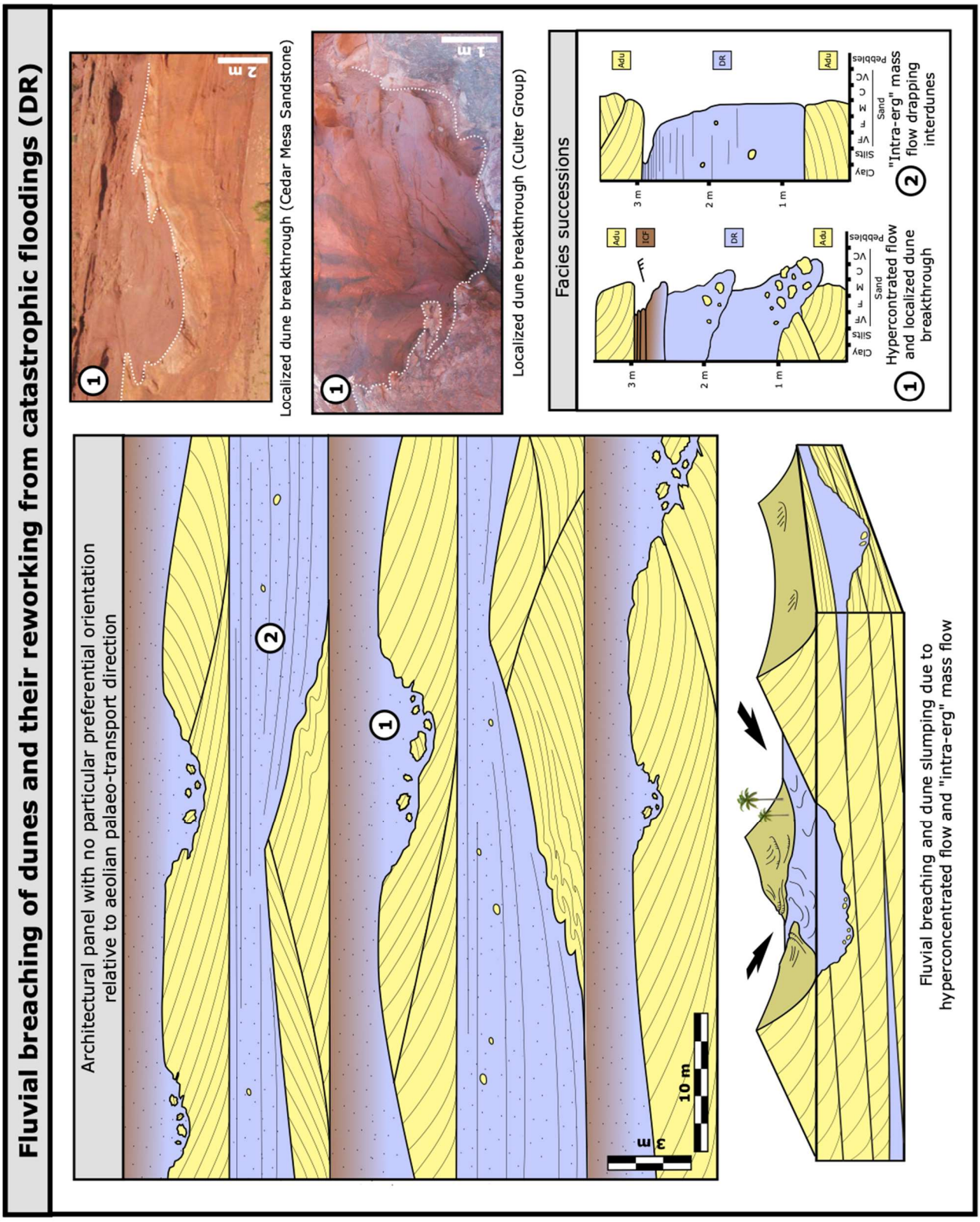


***Figure 10 (2-column fitting).*** *Schematic architectural panel depicting the range of different sedimentary units, elements and geometries symptomatic of catastrophic flooding in dune field (Ahmed Benan & Kocurek, 2000; Svendsen et al., 2003; Cain & Mountney, 2011; Ferronatto et al., 2019). Key features and idealized successions are shown.*

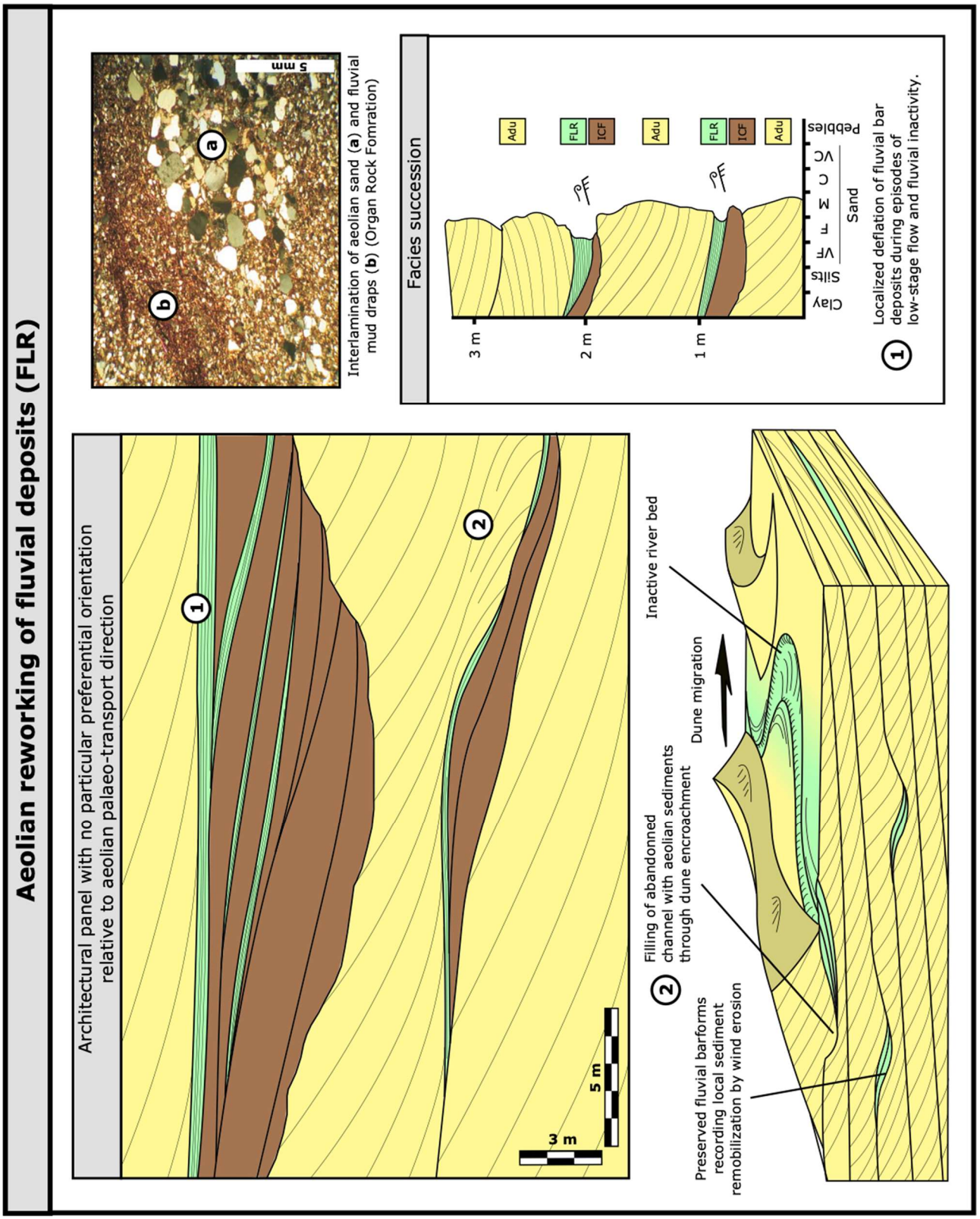


***Figure 11 (2-column fitting).*** *Schematic architectural panel depicting the range of different sedimentary units, elements and geometries symptomatic of fluvial deposits reworked by aeolian processes (Simpson et al., 2008; Cain & Mountney, 2011). Key features and idealized successions are shown.*

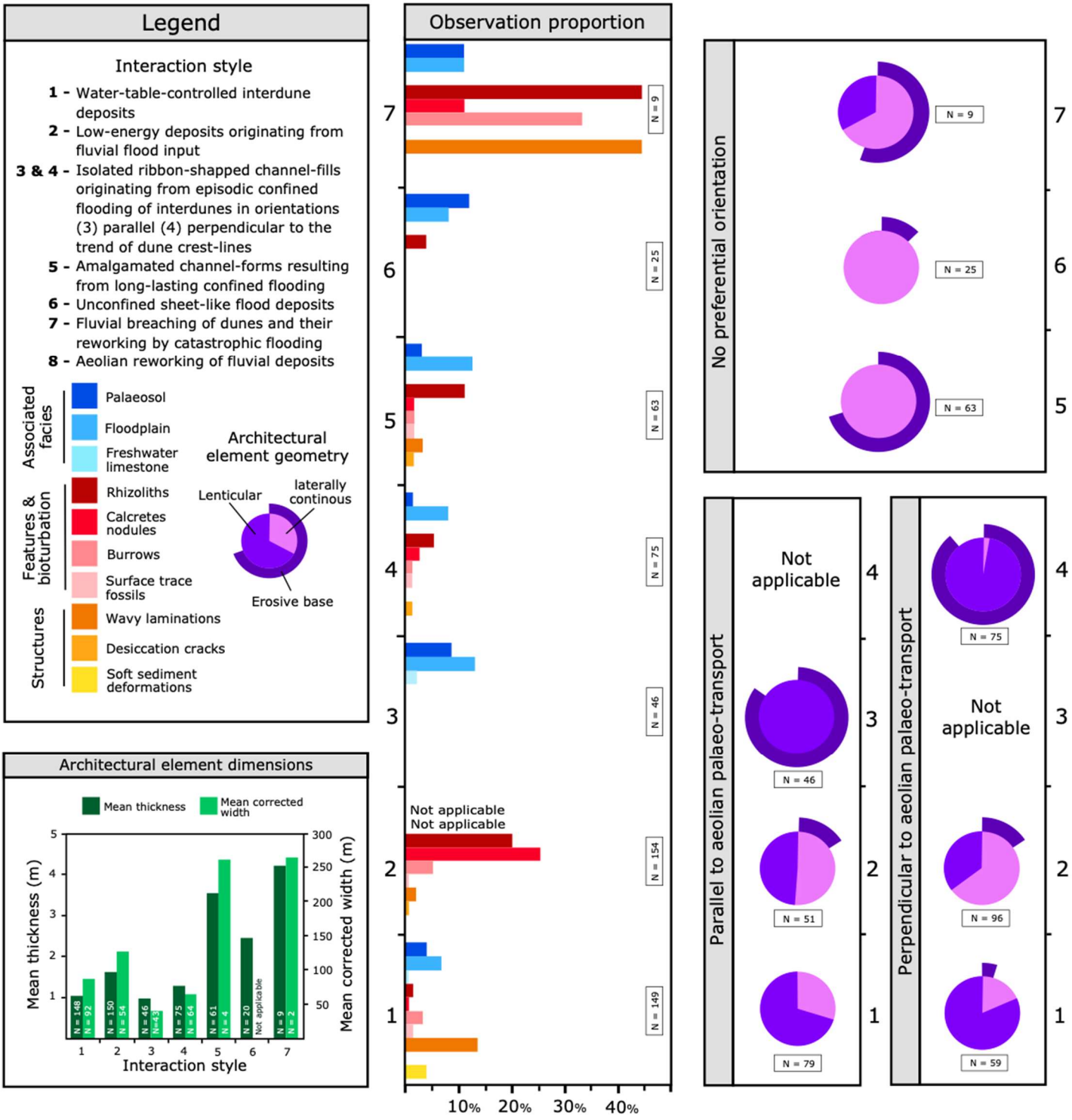


***Figure 12 (2-column fitting).*** *Summary of the range of architectural element dimensions, geometries, boundary types, and diversity of sedimentary features observed in examples of the preserved sedimentary expression of aeolian-fluvial interaction in the Cutler Group. Some primary data used to construct this figure are in part from Jagger (2003), Cain (2009) and Wakefield (2011). Given the generally small scale of observation scale of FLR elements – centimetre to decimetre – no data are recorded in this figure for interaction type 8.*

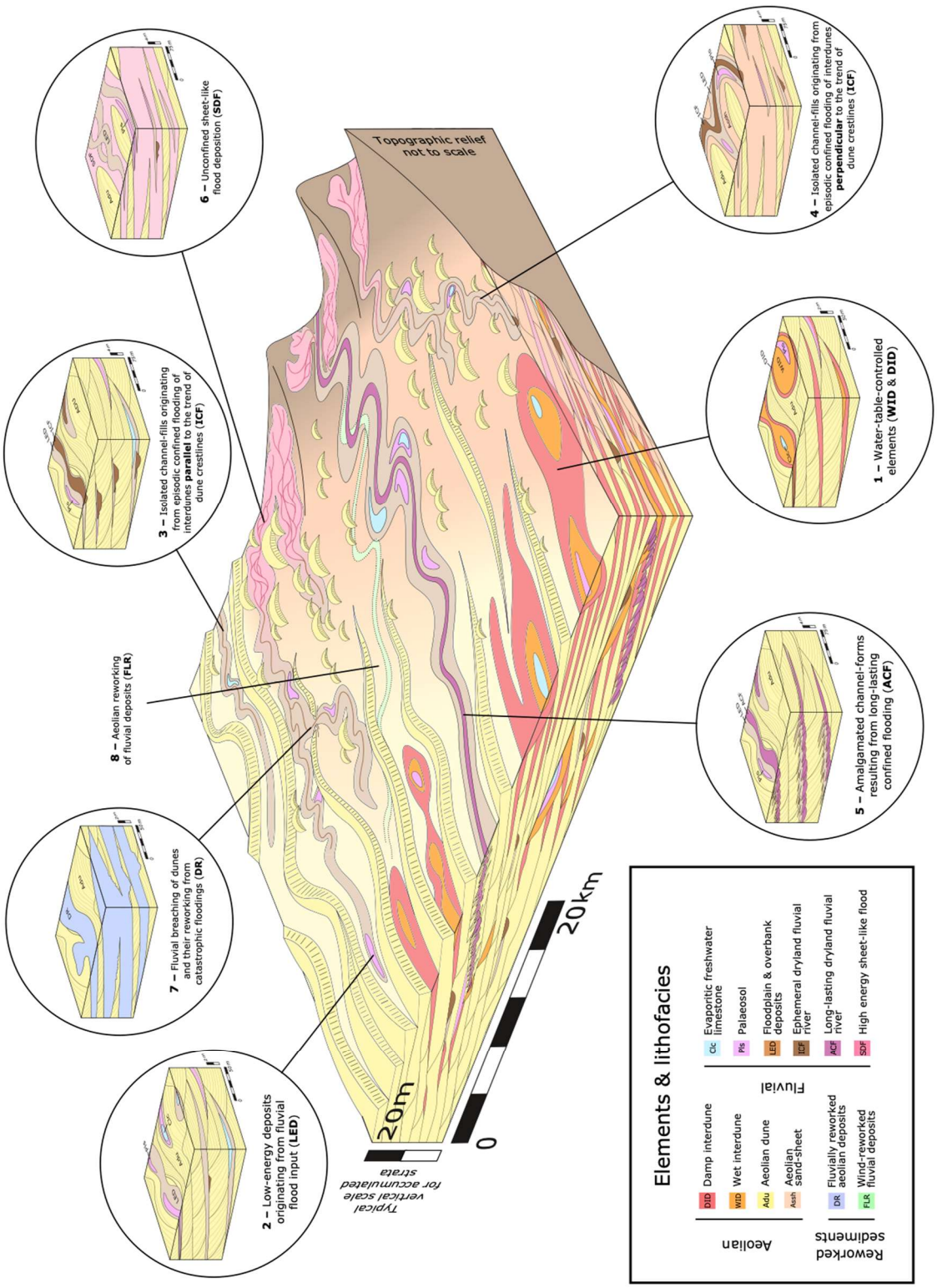


***Figure 13 (2-column fitting).*** *Integrated dynamic facies model for a fluvial-influenced aeolian erg margin displaying different interaction styles between aeolian and fluvial depositional systems with temporal and spatial variations as a consequence of changes in geomorphic controls. Hills, aeolian topographies and fluvial channels are not depicted to scale.*